



estec

European Space Research
and Technology Centre
Keplerlaan 1
2201 AZ Noordwijk
The Netherlands
T +31 (0)71 565 6565
F +31 (0)71 565 6040
www.esa.int

Design, Manufacturing and Testing of a Ball-Head Support, for Thermal Vacuum Chambers Applications

Master Thesis Report
Tesi di Laurea Magistrale
Rapport de Stage PFE
1st June 2019 – 30th November 2019

Candidate:
GROSSO Paola

Company Supervisor:
APPOLLONI Matteo

ENSMA Supervisor:
VIDECOQ Etienne

Politecnico di Torino Supervisor:
GHERLONE Marco

Table of contents:

1	PRESENTATION OF ESA-ESTEC	4
2	INTRODUCTION.....	5
3	LSS ENVIRONMENT	7
3.1	Test centre	7
3.2	Large Space Simulator.....	8
3.2.1	The Vacuum pumping system	8
3.2.2	Shrouds	9
3.2.3	Sun simulator.....	9
4	BIBLIOGRAPHICAL RESEARCH.....	11
4.1	Adhesion, wear and friction	11
4.1.1	Adhesion and cold welding.....	11
4.1.2	Wear and Friction.....	13
4.2	Data.....	19
4.3	Trade-off.....	21
5	PRELIMINARY DESIGN.....	24
5.1	Requirements	24
5.2	Preliminary calculation and analysis	26
5.3	Thermal analysis.....	31
6	JUSTIFICATION	35
6.1	General concept.....	35
6.2	Components description	37
6.2.1	External Case	37
6.2.2	Bottom Plate	37
6.2.3	Sphere	38
6.2.4	Inner ring.....	39
6.2.5	Cylindrical bracket (version A).....	39
6.2.6	Camera Support.....	40
6.3	Installation process and tolerances.....	41
7	MANUFACTURING AND TEST	47
7.1	Test Procedure.....	47
7.2	Test Description and Results	52
8	CONCLUSIONS	56
9	DEFINITIONS AND ABBREVIATIONS	57
10	BIBLIOGRAPHY	58
ANNEX A	: DRAWINGS	62

1 PRESENTATION OF ESA-ESTEC

The European Space Agency, ESA, is an international organisation made up of 22 member states. Established in 1975, its purpose is to shape the development of Europe's space capability.

With an annual budget of 5.27 billion (2019) ESA's programs include: earth observation, navigation, scientific programs, human spaceflight, robotic exploration and more.



Figure 1: ESA Member States and Cooperating States.
Credit: European Space Agency

ESA's facilities are distributed in the following centres:

- EAC, the European Astronauts Centre in Cologne, Germany;
- ESAC, the European Space Astronomy Centre, in Villanueva de la Canada, Spain;
- ESOC, the European Space Operations Centre in Darmstadt, Germany;
- ESRIN, the ESA centre for Earth Observation, in Frascati, Italy;
- ESTEC, the European Space Research and Technology Centre, in Noordwijk, the Netherlands.
- ECSAT, the European Centre for Space Applications and Telecommunications, in Harwell, United Kingdom.
- ESEC, the European space Security and Education Centre, in Redu, Belgium.

Founded in 1968, the European Space Research and Technology Centre is ESA's largest site, with about 2500 engineers, scientists and technicians working on all types of mission design, spacecraft and space technology; it represents the technical and scientific heart of the agency.

ESTEC is also responsible for the testing of spacecraft, its Test Centre is the largest of its kind in Europe, and one of the largest in the world.

2 INTRODUCTION

The Test Centre of the European Space Research and Technology Centre has been using photogrammetry for many years during Thermal Vacuum and Thermal Balance (TB-TV) testing of spacecraft's inside the ESTEC facilities. This is to measure the thermo-elastic deformations that appear in the spacecraft at cryogenic temperatures and under simulated sun illumination.

Scanning photogrammetry system

In 2003 TEC-MXE (Engineering Services Section at Test centre) developed a system of miniaturised space-qualified μ -cameras to improve the operations and performances of thermo-elastic measurements. Flexibility in terms of test set-ups and a remotely controlled motorized scanning system enabled enhancing the system usability and accuracy.



Figure 2: LSS brackets.
Credit: European Space Agency

High Speed Camera System 1st generation

The HSCS is a new camera system that is based on off-the-shelf components and enables better accuracy and faster acquisition. Other advantages are:

- Flexible positioning in the thermal vacuum chamber.
- Reduced costs of COTS (Commercial off-the-shelf).
- Reliable remote operation of the system.
- Simple and thermally stable canister.
- High resolution.
- High-speed frame rate

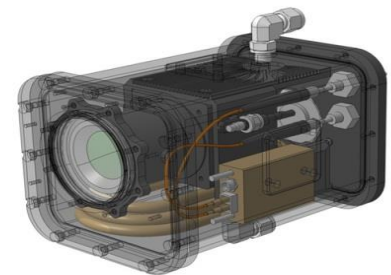


Figure 3: CAD model of HSCS 1st generation.

High Speed Camera System 2nd generation

The latest developments of videogrammetry systems led to a second generation for the High Speed Camera System, which consists of multiple canister-free micro-cameras.

The design of the cameras is based on retro-fitted commercial-of-the-shelf hardware that allows exploitation of commercial cameras advances and therefore brings several advantages:

- Better measurement accuracy
- Faster acquisition
- Small dimensions to reduce contamination

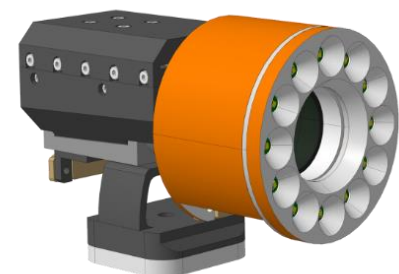


Figure 4: CAD model of HSCS 2st generation.

- Low cost of COTS

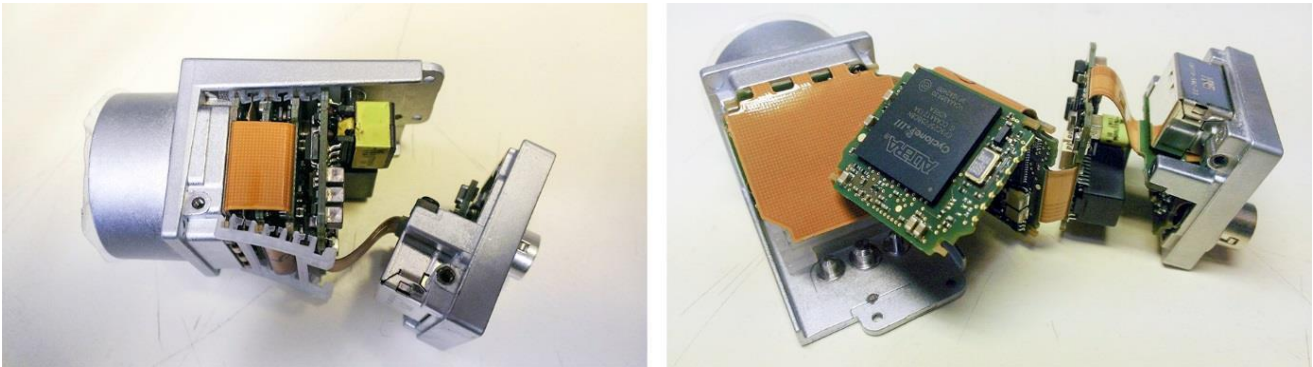


Figure 5: HSCS dismantled.
Credit: European Space Agency

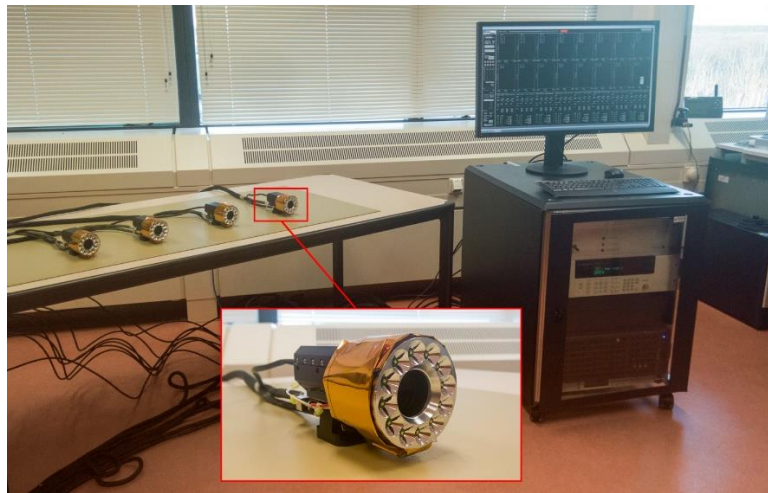


Figure 6: HSCS 2st generation.
Credit: European Space Agency

The cameras (there are eight of them) have to be used in several thermal vacuum chambers, at ESTEC but not limited to.

Within this framework, the design of the mechanical ground support equipment for installation of the cameras in the facilities of the Test Centre is needed.

The objective of this internship is the realisation of a MGSE (Mechanical Ground Support Equipment) for said cameras, by means of a spherical joint, that will need to be still and fixed once inserted in the thermal vacuum chamber, in order to allow the test; but able to move and allow a change on the field of view of the camera once the test is completed, for several cycles of testing. It is necessary not only to design the ball head, but also to follow the manufacturing process and draft a test to be exploited in a small vacuum chamber in order to qualify the product.

3 LSS ENVIRONMENT

3.1 Test centre

The purpose of the test centre facilities and test centre vacuum chambers is to test satellites' and probes' hardware that will be exposed to severe conditions as high vacuum and extremely low/high temperatures due to space environment.

The temperature gradient can easily reach 200°C (+100°C on the surfaces facing the sun, -100°C on those facing deep space); moreover, the vacuum conditions as well as radiation and thermal cycling, play an important role in establishing the lifetime of the spacecraft; hence the necessity of running extensive tests and analysis to be able to predict the behaviour of the spacecraft.

A thermal vacuum test facility must be able to simulate in-orbit conditions in order to confirm that the thermal control as well as all units of the spacecraft (hardware and software) can withstand the harsh space environment, but also to validate its thermal model.

The test centre includes the largest European test facilities such as the Large Space Simulator (LSS), the Large European Acoustic Facility (LEAF), the multi-axis hydraulic vibration facility (HYDRA) and the large electromagnetic compatibility facility (MAXWELL), as well as a number of smaller thermal vacuum chambers and clean rooms.

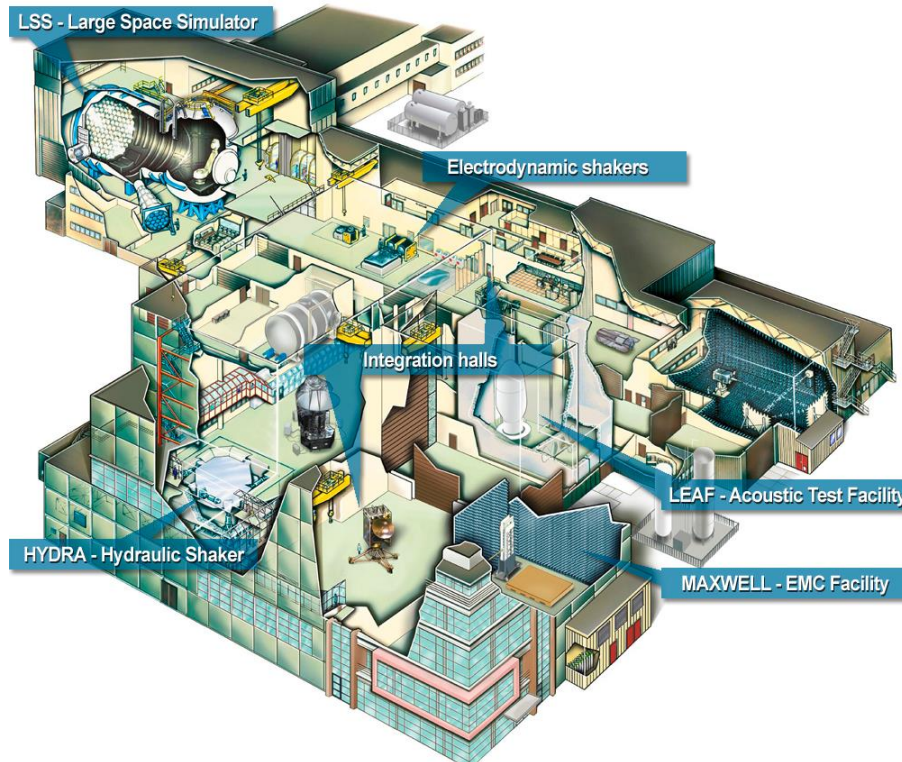


Figure 7: ESTEC's Test Centre.
Credit: European Space Agency

3.2 Large Space Simulator

The Large Space Simulator, with the volume of 2300 m^3 is the largest thermal vacuum chamber in Europe and it has been operative since 1986. It can be considered as the sum of three major parts:

- Main Vacuum Chamber, closed off by a removable lid which consents the load of test objects, and can be accessible from 5m door situated at the bottom level
- Auxiliary Chamber, which contains the cryopumps and the collimation mirror, providing an interface with the solar simulator
- Seismic Block, decoupled from the main chamber via seals, on top of which the test object is mounted with an interface.

Since the purpose of the LSS is to simulate the space environment, there are three main features that characterise the chamber.

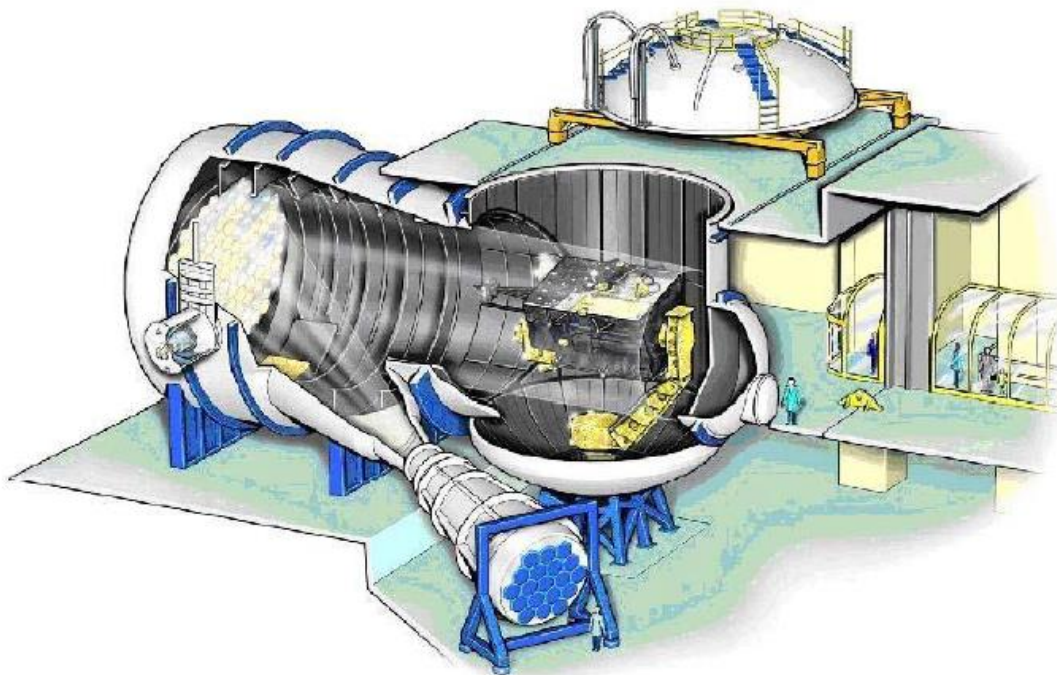


Figure 8: LSS artist's impression.
Credit: European Space Agency

3.2.1 The Vacuum pumping system

The chamber is depressurised by means of two pumping systems: the Central Pumping System (CPS) employed to achieve an initial vacuum level of 5×10^{-3} mbar and a High Vacuum Pumping system (HVP) to reach a pressure lower than 5×10^{-6} mbar, if necessary an additional liquid helium cryopump is available to in the auxiliary chamber to provide additional pumping capability in case of special test requirements. The lowest achievable pressure is 3×10^{-7} mbar.

3.2.2 Shrouds

In order to be able to set a defined temperature the LSS is equipped with a temperature control system made up of the Shroud and Nitrogen Supply Equipment (SNSE). Both the main and the auxiliary chamber are equipped with stainless steel shrouds. The auxiliary chamber's shrouds are kept at a temperature of 77 K using LN₂ (liquid nitrogen) while the ones of the main chamber can either be filled with LN₂ or GN₂ (gaseous nitrogen). The combination of the two allows to bring the chamber to a temperature in the range of 100 K and 353 K.

3.2.3 Sun simulator

The sun simulator system is made up of 19 xenon discharge lamps, each one of them of 25kW of power. An intensity of 1 solar constant (the mean solar electromagnetic radiation of the sun per square meter, measured on the Earth surface, which is approximately $1378W/m^2$) can be obtained by operating 13 of the lamps at the power of 20kW. Before illuminating the spacecraft, the non-filtered xenon spectral radiation produced by the lamps is projected on the collimation mirror, going through an optical integrator via the chamber window.

XENON ARC
LAMP SOLAR SIMULATOR



Figure 9: Xenon arc lamp solar simulator.
Credit: G2Voptics

The light from the stars reaches the Earth perfectly collimated, due to the distance between the objects, the stars present no detectable angular size. As regards the sun, its light reaches Earth uncollimated by 0.5° . The purpose of the collimation mirror is to redirect the beam in order to obtain rays that are as parallel and collimated as the ones reaching the Earth from the sun to reproduce the environment as accurately as possible; it is made up by 109 full segments and 12 half ones.

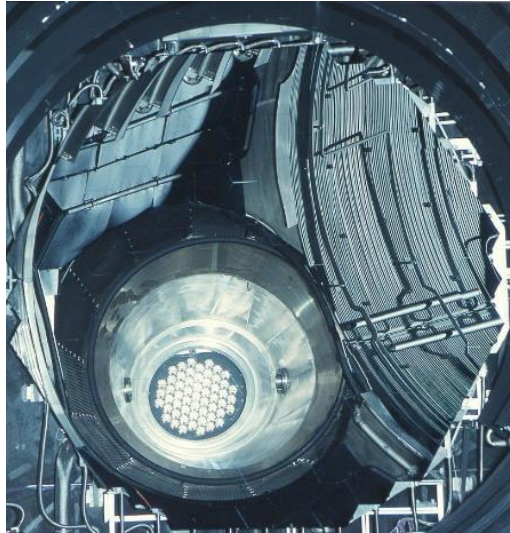


Figure 10: LSS Collimation Mirror.
Credit: European Space Agency

In order to prevent the corruption of the surface, the mirror is thermally controlled via circulation of GN₂ and is kept at a temperature between 26°C and 100°C.

When testing spacecraft that require to get closer to the sun, the intensity level can be heightened by employing all the lamps at the same time, and by equipping the LSS with 32kW lamp and also realigning the mirror to converge the reflected light on the spacecraft and reach up to 8 solar constants,.

The intensity of the beam can be controlled either via manual or automatic settings. During testing, it is also possible to simulate eclipses by placing a shutter between the lamps and the chamber window.

4 BIBLIOGRAPHICAL RESEARCH

One of the earliest and most crucial choices that was made in the process of designing the spherical joint is what materials to employ. Being the working environment of the ball-head a vacuum chamber at cryogenic temperatures, different parameters have been taken into account, such as the amount of wear of the materials over time, the friction coefficient changes when in vacuum and the adhesion behaviour, essential in order to avoid cold welding.

An extended bibliographical research has therefore been carried out.

4.1 Adhesion, wear and friction

4.1.1 Adhesion and cold welding

The term “adhesion” is used in tribology to describe the phenomenon of the formation of bonds between solids.

Adhesion

When two surfaces come into contact, adhesion will occur. [...]

The factors which promote adhesion are:

- Oxide-free surfaces
- Contaminant-free surfaces
- Lubricant-free surfaces
- Similar contact materials
- Inert or vacuum environments

Additionally, the adhesion force is directly proportional to the contact area thus, for a given contact load and geometry, soft materials will adhere more strongly than hard materials (or materials of high elastic modulus).

In general, adhesion between high-modulus materials which are elastically loaded is small.

Adhesion is more likely to become significant if contacts are loaded plastically or are subjected to fretting motion or impact loading. Thus representative testing (e.g. vibration testing followed by functional testing) is imperative to check the integrity of separating surfaces.

Space Tribology Handbook [R1]

The degree of static adhesion forces will depend on a number of factors, such as:

- materials
- loads
- ambient conditions
- temperature

- surface finish
- time of contact
- area of contact
- surface cleanliness

A distinction between autohesion and heterohesion can be defined.

Autohesion indicates the phenomenon of adhesion occurring among different objects made up of the same material, while heterohesion between objects of different materials. Studies about heterohesion are much more complex to carry out the ones about autohesion.

It is essential to take into account the tribological behaviour of mechanical components which are employed under static loads in vacuum for long periods of time, since in vacuum the thin layers of air between objects in contact is not present, “naked” surfaces touch and the threat cold welding between objects is higher. This occurrence must be avoided since the ball head will have to undergo several cycles in the chamber, in between which it will be necessary to change the orientation and position of the camera.

There are different ways to prevent adhesion and cold welding.

One of the most applied solutions is lubrication; for thermal-vacuum applications it is possible to employ both dry and liquid lubricants.

Liquid lubrication can be obtained by the application of one of the three following options: boundary, mixed or fully separated films; while solid lubricants can either be applied as a coating on one of the surfaces in contact, or transferred by rubbing against a body containing or made up by the lubricant.

Nevertheless, the possibility of employing a lubricant was excluded very early in the process, since for a high friction application such as this, even though a lubricant would likely assure the nonappearance of cold welding, it would also reduce excessively the value of the coefficient of friction.

Adhesion has thus to be prevented by means of the choice of materials and by the application of surface coatings; which can also provide a solution to obtain hard-high friction surfaces.

There are different kinds of treatments or coatings that can lead to the production of hard and wear resistant surfaces, they can be classified in thermo-chemical, electrochemical, thermal spraying and vapour deposition by chemical or physical processes (CVD or PVD).

Some of these treatments are compatible with vacuum and cryogenic environment:

- Thermochemical treatments: these treatments employ the phenomenon of solid diffusion in order to modify the chemical composition of the surface layers of alloy, to confer them specific properties as hardness, wear resistance, oxidation resistance and fatigue resistance. The goal is to make the surface absorb a material of different

chemical composition, to confer the surface said properties. Different kinds of thermochemical treatments exist, as: carburising, nitriding, carburation, nitrocarburation. In space environment, the most used are carburising and nitriding; these treatments involve processes at temperatures between 500°C and 900°C. Carburising confers surfaces higher wear and fatigue resistance, while nitriding, definitely the most used in space applications, creates a thin layer (5 microns) with very high hardness (1500 Hv) supported by a thicker layer that is nitrogen-enriched. Disadvantages lie in the risk of modifying the component because of the high temperature employed in the process.

- **Anodization:** this treatment consists in enhancing the natural layer of oxide that can be found on the surface of Aluminium and Titanium alloys, through the immersion of the component in an acid solution and application of continuous current and the component, employed as the anode, is covered by an oxide layer, which growth's can be controlled, because the oxygen developed via of the current combines with the substrate material. For Aluminium alloys, hard anodising is the most applied procedure and it creates a superficial oxide layer with a thickness between 25 and 100 microns.
- **Hard chrome plating:** this kind of treatment belongs in the electro-chemical group, and it's used to improve hardness and wear resistance of Titanium and Aluminium alloys. The electro-chemical process of deposition is carried out soaking the component into a chrome-sulphur electrolyte, after the oxide layer has been removed. During the process the temperature is usually set between 50°C, 60°C and the final thickness of the layer of about 75 microns, thinner coatings would crack spontaneously while thicker ones could experience microcracking and become permeable. This kind of treatment has been used in space application, often accompanied by sputtered MoS₂.
- **Vapour deposition treatments:** ceramic coatings can be applied via CVD and PVD in order to obtain hard and high friction surfaces. CVD processes can be employed to apply diamond or TiC coatings, this method is based on the decomposition of the coating material in gas at the temperature of 100°C. PVD techniques relay on the volatilization of in a low-pressure chamber by either heating or ions bombardment, creating a thin hard and brittle layer, these work best if employed on a hard substrate, as steel. During these processes the component is subjected to lower temperatures than in thermochemical treatments. Examples of coatings that can be applied via PVD or CVD are TiN, CrN, TiCN or WC.

4.1.2 Wear and Friction

Tribometry is the science that deals with friction and wear phenomenon; to obtain data in these regards, *tribometers* can be employed, these are devices used to measure friction forces or friction coefficients.

Wear can be defined as the damaging, deformation or loss of a material at the surface of an object, which has, consequently, its deterioration or the worsening of its initial physical properties.

Wear may occur due to different reasons, for example:

- **Adhesion:** adhesion wear is a very dangerous form of wear, since it progresses quickly and leads to the friction coefficient becoming instable. Surfaces in contact that slide onto each other, can be quickly damaged by this kind of wear, especially if a lubricant is not employed and direct contact is present, because asperities in the materials surfaces might weld at the tips and material is transferred from the softer to the harder material.

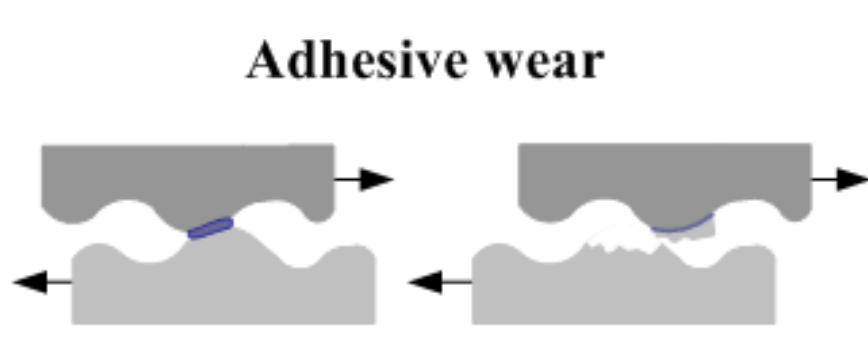


Figure 11: Adhesive wear phenomenon.
Credit: [R5]

- **Fatigue wear:** another type of wear is seen even if surfaces are well lubricated, this phenomenon is caused by the deformations that the asperities of the surfaces undergo in time, when the contact under high loads repeats for several cycles. The higher the load, the lower the number of cycles is necessary to experience wear. The particles that are released in this kind of wear, may lead to creep growth and propagation, and determine, over time, the failure of the component.
- **Corrosion and oxidation wear:** the main cause of this kind of wear is the reaction between the surface and environment, the most common corrosive attack is identified in oxidation. In some cases, it leads to the formation of a hard layer that fights wear and guarantees low friction, but if this layer breaks off, wear may appear due to particles release. This type of wear doesn't appear in vacuum.
- **Cavitation wear:** cavitation is characterised by the cyclical development and collapse of gas bubbles on a solid surface in contact with a fluid. These bubbles form if the pressure in the fluid drops (it can appear for example in aeronautical engines). The collapse of the bubbles near the surface generates high stresses that can damage the surface of the solid, causing cavities in softer materials and fracture or fragmentation in the harder ones.

- Erosion wear: it is caused by the impact of solid or liquid particles on the surface of an object. It includes different mechanisms that derive from the type of material that the particles are made from, the angle and speed of impact, and the dimension of the particles.
- Other kinds of wear include plastic deformation wear, melting wear, cutting or tearing wear.

Even though wear is more commonly associated to metallic materials (metals and their alloys) it can affect many types of materials.

Employing a quantitative theory, it is possible to define a relation between wear and the relative area of contacts between two surfaces. Defining V the volume affected by wear and L the sliding distance that causes it; a wear rate can be defined as V/L , with dimensions of an area

$$\frac{V}{L} = K \times A = K \frac{W}{p_m}$$

Where:

- W is the normal contact load,
- p_m is the mean contact pressure,
- K is defined as the non-dimensional wear coefficient.

If the value of K is too high ($K > 10^{-2}$), the system is considered inadmissible for engineering processes.

Wearing Surface	Counter Surface	Wear Rate (10-6mm³/m)	Hardness (HV)	Mean Friction Coefficient	Wear Coefficient K
Mild Steel	Mild Steel	1.57×10^4	186	0.62	7×10^{-3}
Leaded Brass	Tool Steel	2.4×10^3	85	0.24	6×10^{-4}
PTFE	Tool Steel	2.0×10^2	5	0.18	3×10^{-5}
Stellite	Tool Steel	32	690	0.60	6×10^{-5}
St. Steel	Tool Steel	27	250	0.53	2×10^{-5}
Polythelene	Tool Steel	3	17	0.53	2×10^{-7}
WC	WC	0.2	1300	0.53	2×10^{-6}

Table 1: Unlubricated Wear Rates and Friction Coefficients for Various Materials (in air, crossed cylinders test configuration).

Credit: [R1].

It's also possible to express the wear rate as the quantity of material removed, per time or per unit distance of sliding, which means that it will be proportional to the force. Indicating k as the specific wear rate in $\frac{m^3}{Nm}$

$$\frac{V}{L} = kW$$

During a test, wear is usually measured as the change in volume and geometry or mass. To calculate k it is assumed that wear is proportional to the load, so it is commonly expressed as the volume removed in sliding distance and load unit; while for K it is only necessary to know the worn volume and the total sliding distance.

Test faces are normally classified as shown in figure 12:

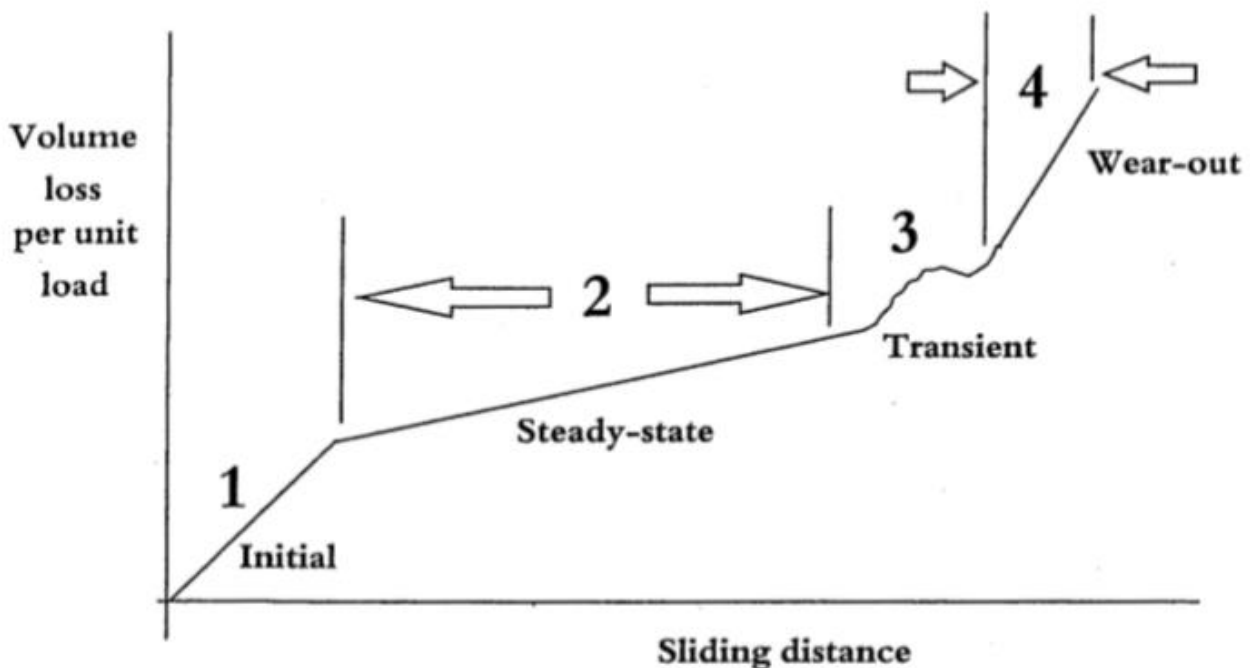


Figure 12: Output of a general wear measurement.
Credit: [R1].

1. Initial: wear rate at the beginning of the test.
2. Steady state: relatively long period of time where the wear rate can be considered constant.
3. Transition. Instantaneous change in wear rate, usually because of a change in the dominant wear mechanism.
4. Wear-out. Wear at the end of the test.

Tribology is not an exact science, it is not possible to define a precise value of friction for a certain material coupling, the outcome depends on the test conditions, and it will be a spread of results.

In general, the output of a tribometer is a signal that connotes friction force, measured continuously, as a function of time, which is normally denoted as test duration as in time, sliding distance or number of cycles. It is important to consider time because friction and

wear both depend on it, again, as it was done for wear, it is possible to classify test faces as shown in figure 13.

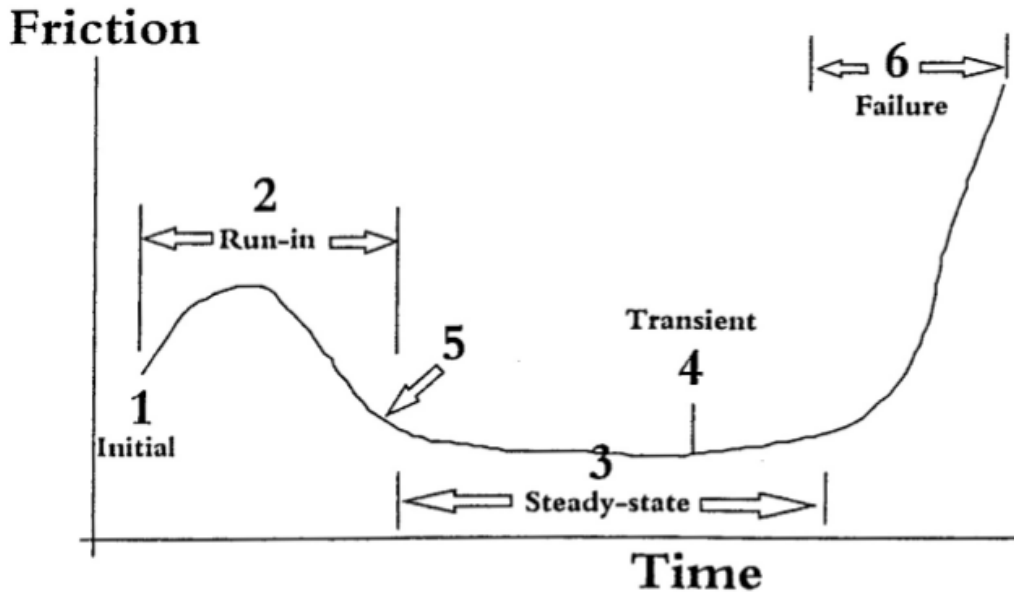


Figure 13: Output of a general friction measurement.
Credit: [R1].

Where:

1. Initial: friction at the beginning of the test.
2. Run-in: friction at the early stages of the test.
3. Steady-state: friction for most of the test, the value is basically constant.
4. Transient: sudden change in friction.
5. Instantaneous: in general, point value of friction at any time.
6. Failure: friction at the end of the test, usually it's the highest value of friction.

A general tribometer scheme is shown in figure 14, to be able to measure friction coefficient, both loaded contact between two surfaces and its measurement of the contact load are necessary.

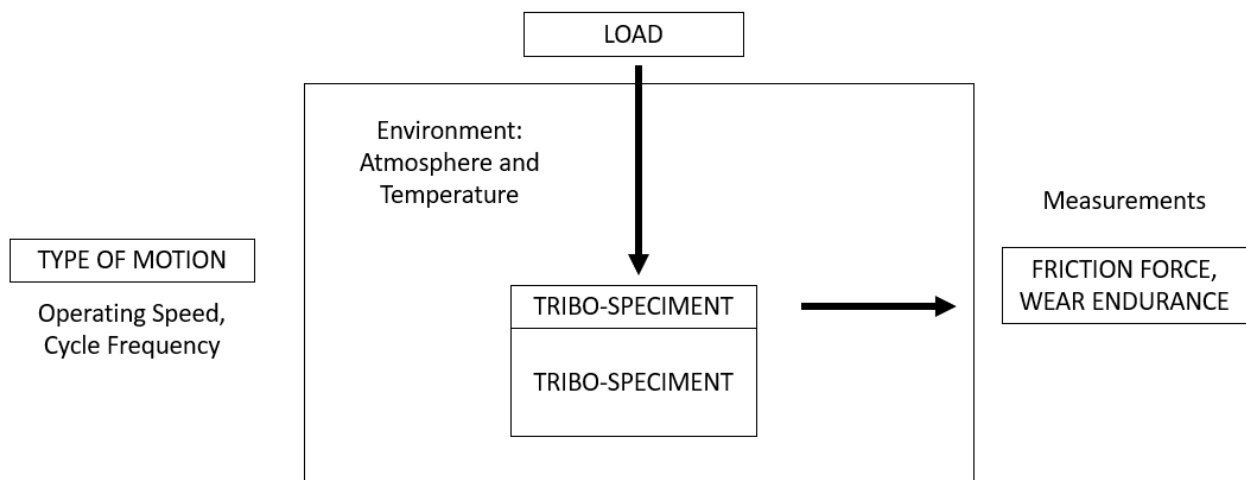


Figure 14: Generic tribometer set up.

Tribometers can be classified based on the contact type and motion type but, especially for space application, also temperature and atmosphere need to be taken into account.

Pin-on-disc: it's a setup which employs a pin or a ball sliding against a disc or a flat surface. The motion can be unidirectional or reciprocal between the two objects. This kind of test is used to measure kinetic friction coefficients as well as wear rates. It can also allow the determination lubricant lifetime.

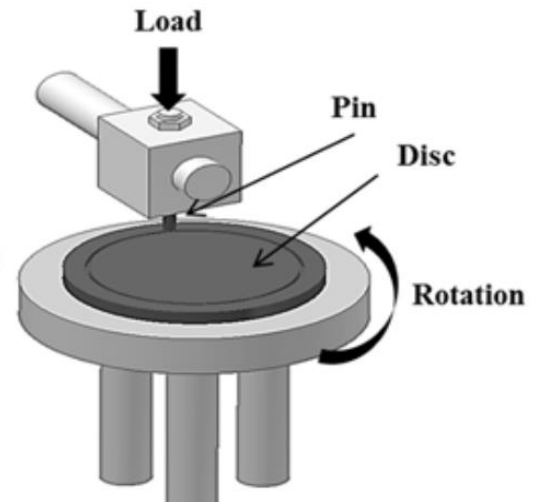


Figure 15: Pin-on-disc setup.
Credit: [R31]

Two-disc: in this configuration, two discs are positioned parallel to each other, on shafts rotating on opposite directions. The shafts can rotate at different speed in order to evaluate different characteristic when sliding or during slip motion. It is mainly used to understand friction and wear in different conditions of sliding and rolling contact.

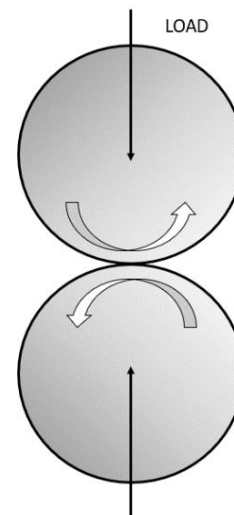


Figure 16: Two-disc setup.

Four-ball: this setup is made up of four balls positioned in a tetrahedron configuration. The upper ball is the only one that rotates, while the lower ones are fixed. It is mainly used to measure high pressure contact properties and load carrying capacities of lubricants.

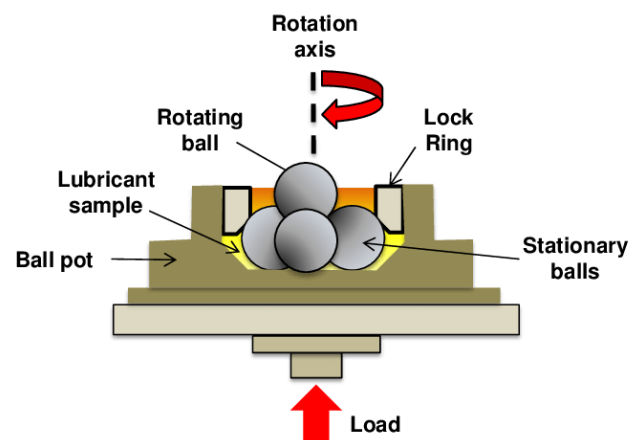


Figure 17: Four-ball setup. [R20]

4.2 Data

Once a general research on the tribometrical aspects of working in vacuum-cryogenic environment was carried out, the research continued with high friction space applications, and the materials that have been used throughout the years.

Even though several high friction mechanism applications in space environment can be found in literature, only a few are meant to prevent motion at the interface of the surfaces.

Table 2 shows the main couplings found in literature that could be suited for the spherical joint application:

Contact material combination	Surface treatments or coatings	References
455 stainless steel (counter face not specified)	TiC	R21
410 stainless steel vs. Al 7075	No treatment specified	R10
Ti alloy vs. Z10 CNT 18-11	PVD TiN or TiC on Ti alloy	R23
Ti alloy	Hard Chrome	R14
Ti alloy	TiN coatings and lubricant	R24
Ti alloy	Anodisation with included PTFE and Braycote 602	R4
Vespel SP3 vs. stainless steel or Al alloy	No treatment specified	R29
Vespel SP3 vs. Al alloy	Al-alloy hard Anodised	R22
Al-alloy vs. Al alloy	One surface hard anodised and lubricant Braycote 601	R17
Al alloy	Hard anodisation or Keronite coatings	R9

Table 2: High friction material coupling possibilities.
Credit: [R2].

As a preliminary design was drafted, it was decided that the core of the mechanism would be made up of 3 parts: a sphere, an inner ring encasing the sphere, and an outer case to contain the other two parts, with the function of keeping the parts in place and of applying the load necessary to prevent the movement and therefore keep the camera in a fixed position to allow the test, as shown in figure 18.

These three parts are pressed together, to fix the position of the camera, by means of a bolt inserted in the outer case, hence they're subjected to high loads and they are likely to undergo adhesion, unless precautions are taken to avoid it.



Figure 18, preliminary concept of the joint.

Among the options listed in table 2, three were identified as possible candidates to be employed; the others were excluded either because of the necessity to apply lubricants, which as previously discussed in chapter 3 are going to be avoided, or because of the type of coating or bulk material.

The three selected couplings are:

- 410 stainless steel vs. Al 7075
- Vespel SP3 vs. Al alloy
- Al alloy vs. Al alloy (both hard anodised)

Vespel SP3 is a durable high-performance polyimide-based plastic, the main properties are listed in Table 3:

Property	Vespel SP3
Filler Material	15% Moly (MoS ₂)
Density	1.60 g/cm ³
Elongation at break, 23°C	4.0

Flexural Modulus, 23°C	3280 MPa
Flexural Modulus, 260°C	1860 MPa
Compressive Stress at 10% strain, 23°C	128 MPa
Deformation under 13.8 MPa load	0.12
Hardness, Rockwell	E40-55
Coefficient of Linear Thermal Expansion	52 $\frac{\mu m}{mK}$

Table 3: Vespel SP3 main properties.
Credit: DuPont

A trade-off approach was employed to choose the most fitting coupling for this application.

4.3 Trade-off

Table 4 summarizes the trade-off made between the three possibilities.

The selection was made based on 9 criteria, which importance was valued between 1 (marginal) 2 (fairly important) and 3 (important) to the design.

Each coupling was assigned a “score” for every criterion, based on how well said criteria is satisfied. The “scores” are assigned from - - to + +, each of them is then multiplied by the number in the last column, and summed column by column to obtain a total.

	Criteria	410 stainless steel versus Al 7075	Al alloy versus Al alloy both hard anodised	Vespel SP3 versus Al alloy hard anodised	1-3
1	Vacuum materials compatibility	++	++	++	3
2	Cryogenic compatibility	++	++	++	3
3	Low wear	--	0	++	3
4	Cold welding avoidance	+	0	++	3
5	Thermal deformation	+	++	0	2

	<i>compatibility</i>				
6	<i>Friction</i>	+	+	+	3
7	<i>Outgassing</i>	++	++	++	2
8	<i>Machinability</i>	++	++	++	1
9	<i>Cost</i>	++	++	--	1
	TOT	22	27	31	

Table 4: Material trade-off.

The purpose of table 5 is to explain how the evaluation of every coupling was chosen.

		Choice justification	410 stainless steel	Al alloy (7075 Al)	Vespel SP3
1	<i>Vacuum compatibility</i>		✓	✓	✓
2	<i>Cryogenic compatibility</i>	T range	✓	✓	-195°C - 350°C
3	<i>Low wear</i>	Reference document	✓	✓	✓
4	<i>Cold welding avoidance</i>		✓	Same material, likely undergo strong adhesion	✓
5	<i>Thermal deformation</i>	Coefficient of thermal expansion	$9 - 11 \frac{\mu m}{mK}$ vs $21 - 24 \frac{\mu m}{mK}$	Same: $21 - 24 \frac{\mu m}{mK}$	$52 \frac{\mu m}{mK}$ vs $21 - 24 \frac{\mu m}{mK}$
6	<i>Friction</i>		✓	✓	✓
7	<i>Outgassing</i>		✓	✓	✓
8	<i>Machinability</i>		✓	✓	✓

Table 5: Justification of the material trade-off.

The coupling selecting with the trade-off was Vespel SP3 versus Al 7075 hard anodised.
The inner ring is made in Vespel SP3, while the outer case and the sphere in Al 7075.

5 PRELIMINARY DESIGN

5.1 Requirements

In the following paragraph, functional, interface, environmental and design requirements will be described.

FUNCTIONAL AND PERFORMANCE REQUIREMENTS	
ID	Description
FPR-1	The mechanism of the MGSE shall not move after its position has been fixed, in any of the working conditions described by ER-1
FPR-2	The MGSE shall allow 2 degrees of freedom (azimuth and elevation rotations) for the pointing of the cameras.
FPR-3	The MGSE shall allow elevation angles within range of approximately 45 degrees.
FPR-4	The MGSE shall allow azimuth angles within range of approximately 15 degrees.

Table 6: Functional and Performance Requirements.

INTERFACE REQUIREMENTS	
ID	Description
IR-1	The MGSE shall be thermally decoupled from the shrouds of LSS.
IR-2	The MGSE shall be thermally decoupled from the HSCS (High Speed Camera System).
IR-3	The MGSE shall be compatible with existing LSS installations.
IR-4	The MGSE shall be compatible with the mechanical interface of HSCS.

Table 7: Interface Requirements.

ENVIRONMENTAL REQUIREMENTS	
ID	Description

ER-1	<p>The support equipment shall be used under the following operational conditions:</p> <ul style="list-style-type: none"> - Temperature: 100 to 300 K - Relative Humidity: 40% to 60% - Pressure: $3 \cdot 10^{-7}$ mbar - Clean room: Class 100.000
ER-2	The system shall be built as to minimize thermal and particle pollution.

Table 8: Environmental Requirements.

DESIGN REQUIREMENTS	
ID	Description
DR-1	The support equipment shall be designed to accommodate harness of the cameras.
DR-2	The system shall be built such as to ease quick installation, meaning that the installation of the eight cameras should be carried out within one day.
DR-3	The MGSE shall be designed considering the minimization of costs and complexity of its potential procurement/implementation.
DR-4	The MGSE shall be as light and compact as possible.
DR-5	The MGSE shall be designed to ease and minimize maintenance activities.
DR-6	The MGSE shall have a lifetime of at least 10 years.
DR-7	The MGSE shall be designed to include safety mechanism in case of failure of the primary installation mechanism.
DR-8	The MGSE shall be easily handled and operated.

Table 9: Design Requirements.

5.2 Preliminary calculation and analysis

Once the materials have been selected, preliminary calculations are run on an early design in order to evaluate loads and toques involved.

The preliminary design of the MGSE includes two different brackets to hold the camera, which can be exchange by mounting and dismounting them, based on the type of application.

The first version of the MGSE, mounted with the long cylindrical bracket, is illustrated in figure 19. A long cylindrical bracket is employed for two reasons.

Firstly, it is necessary for the camera to be distant enough from the wall to enable the accommodation of the harnesses that will be connected to it. The hooks are used to connect the MGSE to a rod in the LSS (configuration a).

Secondly in case necessary, this version allows the MGSE to be positioned on a table or a flat surface (configuration b). This second configuration provides also a safe and compact way of transportation for the MGSE when needed.



Figure 19: Employment of the long cylindrical bracket. a. MGSE connected to the LSS (on the left) b. MGSE placed on a flat surface (on the right).

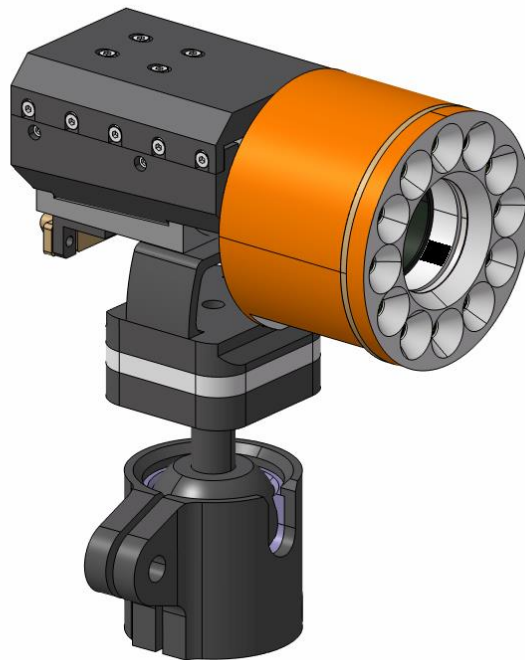


Figure 20: Employment of the short cylindrical bracket.

A short cylindrical bracket has been designed to have a lighter and simpler MGSE for the camera in case it needs to be mounted on a regular tripod.

To evaluate the torque necessary to be applied on the spherical joint to keep it in position, the calculations are based on the second type of bracket in order to be conservative, since the overall length is bigger, the lever and so the torque to apply are larger as well.

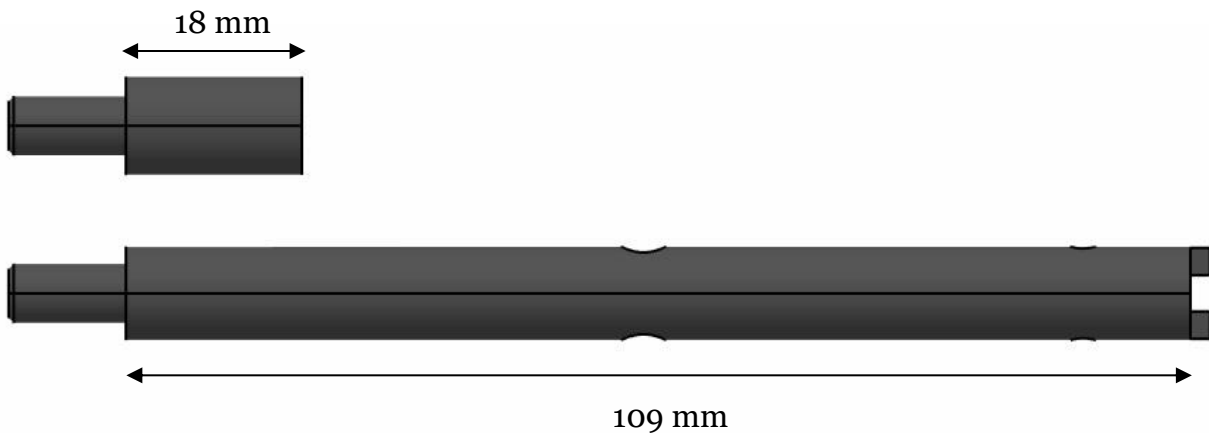


Figure 21: Dimension of the cylindrical brackets.

To understand the forces involved, the assembly was modelled as a beam clamped on one end, as in figure 22:

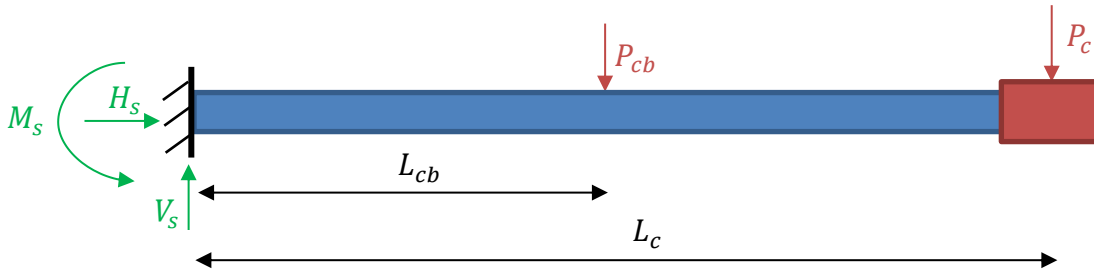


Figure 22: Schematisation of load on the spherical joint.

	Definition	Value
P_c	Weight of the camera and camera harness	4.05 N
P_{cb}	Weight of the cylindrical bracket	0.34 N
L_c	Lever of the camera	0.18 m
L_{cb}	Lever of the cylindrical bracket	0.067 m
M_s	Torque at the clamp	0.752 Nm
H_s	Horizontal constraint reaction force	0 N
V_s	Vertical constraint reaction force	4.395 N

Table 10: Data and results of preliminary calculations.

This preliminary calculation shows that to balance the forces applied, and so prevent the movement of the sphere, a torque of 0.752 Nm must be applied on the ball head.

In order to measure the value of the force to apply on the thread, it is necessary to take into account the friction between Vespel SP3 and the aluminium alloy Al7075. Since no record of the value of the friction coefficient between the two materials was found in literature, an assessment was made in order to define a conservative value for it, to be able to calculate the forces involved in the system.

From the Vespel SP3 properties sheet we can find table 11 and figure 23.

Table 11 shows the value of the kinetic friction coefficients of Vespel SP3 versus carbon steel, in steady state, unlubricated, in air environment, thrust bearing:

PV (pressure-velocity loading)	Coefficient of friction
$0.875 \text{ MPa} \frac{\text{m}}{\text{s}}$	0.25
$3.5 \text{ MPa} \frac{\text{m}}{\text{s}}$	0.17

Table 11: Kinetic friction coefficients of Vespel SP3 versus carbon steel, in steady state, unlubricated, in air environment, thrust bearing.

Also, qualitative information can be found in figure 23.

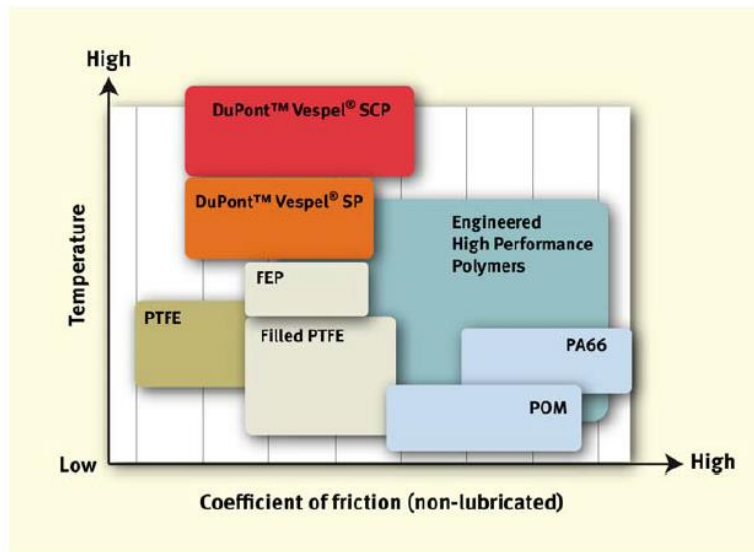


Figure 23: Vespel friction coefficient compared to other polymers.
Credit: DuPont

Based on literature research, the static friction coefficient of PTFE against Al7075 has a value of 0.19.

The static friction coefficient is generally higher than the kinetic one, since overcoming static friction means prevail over molecular and mechanical obstacles that are present at the interface between the two objects (static friction is caused, in most cases, by adhesion and abrasion at the contact points); while when the movement is already initiated, even though the obstacles are still present, abrasion will occur again, but at lower intensity. Also, due to inertia the amount of energy required to keep an object in movement is lower than the one necessary to initiate motion.

As shown in figure 15, the friction coefficient of the Vespel SP series, is higher than the PTFE's. Combining all these data, the static friction coefficient between VespelSP3 and Al 7075 was chosen as 0.17, in order to be conservative.

To evaluate the momentum to be applied on the bolt, it is first of all necessary to calculate the normal force F_N and tangential force F_T to be exerted on the sphere.

$$M_s = F_T r = F_N r \mu_s$$

Where:

- r is the radius of the sphere $r = 15 \times 10^{-3} \text{m}$
- μ_s is the static friction coefficient between VespelSP3 and Al7075 $\mu_s = 0.17$

$$F_N = \frac{M_s}{\mu_s r} = 295 \text{ N}$$

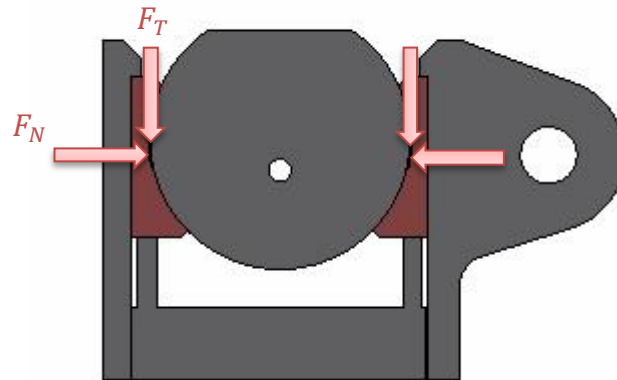


Figure 24: Cross section of spherical joint and friction forces.

Once the normal force to exert on the surface of the sphere has been calculated, it is possible to determine the load to apply on the bolt.

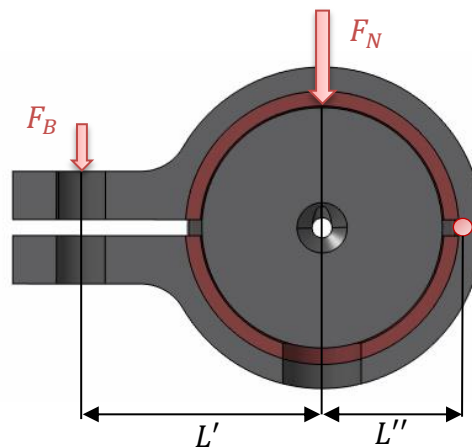


Figure 25: Cross section of spherical force and applied force.

The external case can be modelled as a lever, where the fulcrum is indicated by the red dot in figure 25. In order to obtain the load F_N on the sphere, a force F_B must be applied at the bolt, and it can be calculated as follows.

$$F_B = \frac{L''}{L'} \times F_N = 167 \text{ N}$$

Where L' is 30 mm and L'' 17 mm.

To determine the tightening torque to apply on the bolt, the following formula can be used.

$$M_B = fDF_B$$

Where:

	Definition	Value
f	friction coefficient (nut factor)	0.2
D	bolt's nominal diameter	6 mm (M6 bolt)
F_B	desire tensile load	167 N

Table 12: Definition of parameters to calculate the torque to apply on the bolt.

$$M_B = fDF_B = 0.2 \times 6 \times 10^{-3}m \times 167 N = 0.2 Nm$$

In this preliminary calculation, M_B is defined as the torque to be applied on the bolt in order to obtain the load necessary to fix the sphere, given that the surfaces of the three parts are in contact. For mounting purposes, it will be necessary to have play between the parts, defined through tolerances in the design that will be discussed and described in the following chapters.

This means that an additional compression load will be needed, the final tightening torque value will be higher than 0.2 Nm.

5.3 Thermal analysis

A simple thermal analysis needs to be implemented to ensure the consistency of performance of the clamping mechanism once the MGSE is inserted in the LSS, since inside the chamber the temperature of 100K is reached.

Due to the heat irradiated from the camera and harnesses and the action of isolating brackets the lowest temperature reached by the ball head would be 150K but these analysis are carried out considering 100K, in order to be conservative and take into account the worst case. Moreover, coefficients of linear thermal expansion are considered constant and tolerances are not considered, as they will be analysed in the following chapters. All the measures shown in the following chapter are the nominal ones.

In figure 26, the section drawing of the spherical joint shows the nominal dimensions at ambient temperature ($T = 293.15K$).

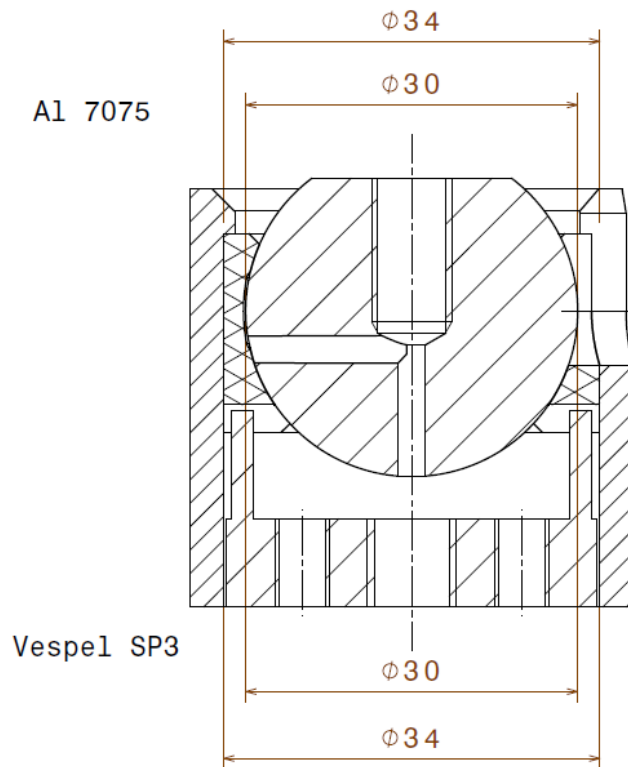


Figure 26: Cross section of spherical joint at T=293.15K.

Since the internal case is not built as an individual piece but made up of two halves, as shown in the following figure, it is possible to analyse separately the external case and sphere (made in Al 7075) and the internal ring (Vespel SP3)

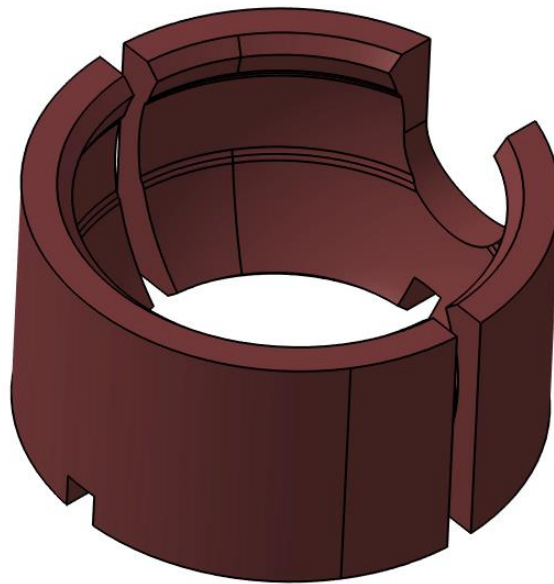


Figure 27: Inner ring in Vespel SP3.

The external case and the sphere, being both made of Al7075, have the same coefficient of linear thermal expansion ($CTE_{Al7075} = 22.5 \frac{\mu m}{mK}$).

The dimensions in cryogenic have been calculated [R13]:

$$D = D_0 - D_0 CTE_{Al7075} \Delta T$$

Where $\Delta T = 293K - 100K = 193K$

$$D_{sphere} = 30mm - 30mm \times 22.5 \frac{\mu m}{mK} \times 193K = 29.8697mm$$

$$D_{external_case} = 34mm - 34mm \times 22.5 \frac{\mu m}{mK} \times 193K = 33.8523mm$$

$$D_{Al7075} = D_{external_case} - D_{sphere} = 3.9826 mm$$

As regards the inner ring, the Vespel SP3 has a higher coefficient of thermal expansion ($CTE_{vespelSP3} = 52 \frac{\mu m}{mK}$), the dimension at 100K can be calculated in the same way:

$$D = D_0 - D_0 CTE_{vespelsp3} \Delta T$$

$$D_{out} = 34mm - 34mm \times 52 \frac{\mu m}{mK} \times 193K = 33.6588mm$$

$$D_{in} = 30mm - 30mm \times 52 \frac{\mu m}{mK} \times 193K = 29.6989mm$$

$$D_{vespelsp3} = D_{out} - D_{in} = 3.9599 mm$$

The overall gap generated becomes:

$$D_{gap} = D_{Al7075} - D_{vespelsp3} = 23\mu m$$

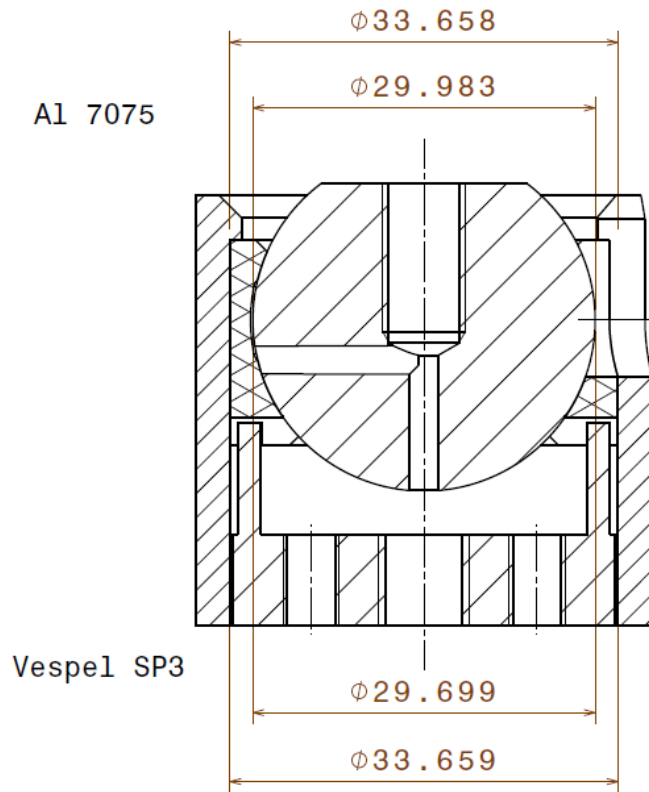


Figure 28: Cross section of spherical joint at T=100 K.

When the chamber reaches cryogenic temperatures, an overall play of $23 \mu\text{m}$ is generated; even though this gap is very small, it will be taken into account when dimensioning the tightening torque to be applied on the ball head.

6 JUSTIFICATION

In this chapter the spherical joint will be analysed component by component in order to explain how the design choices were made. The complete drawings of each component can be found in Annex A.

6.1 General concept

The final version of the spherical joint and support parts is shown in figure 29.

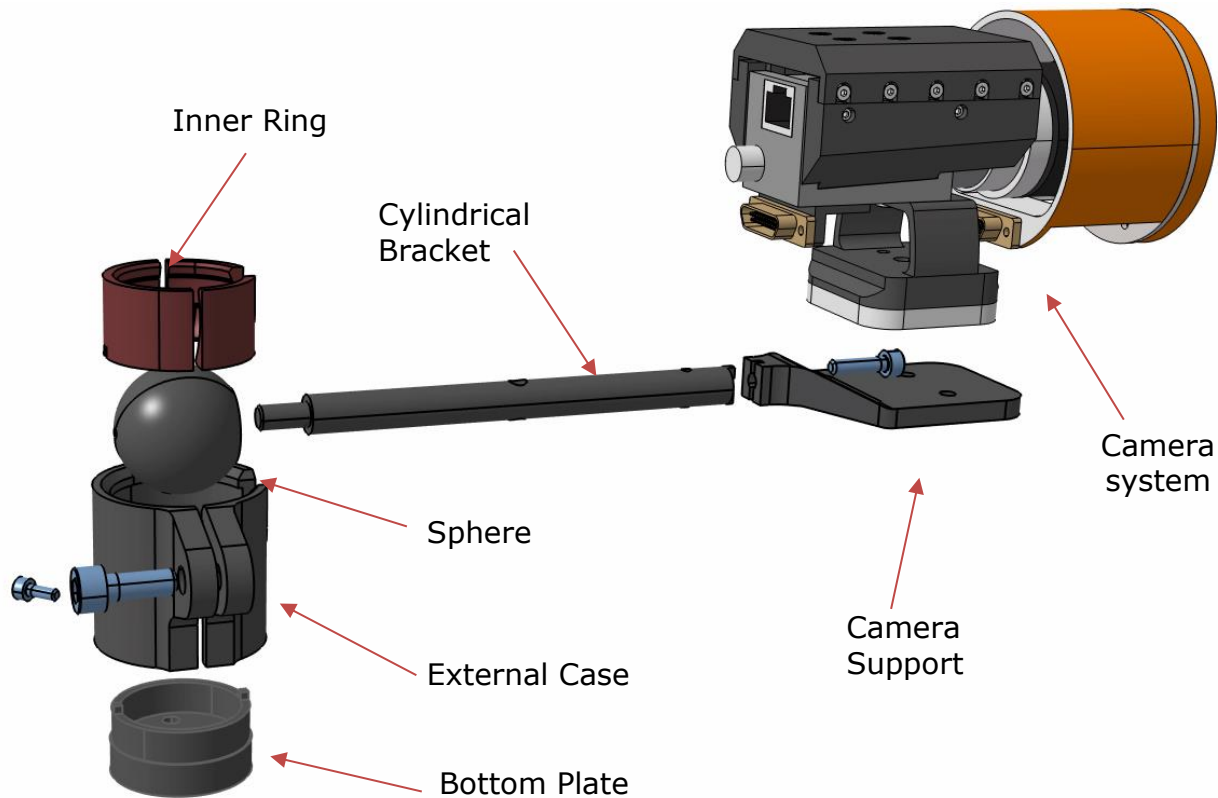


Figure 29: Spherical joint and support parts: exploded view.

A description of the function of each component is shown in table 13.

Element	Quantity	Function
Bottom Plate	1	Supports the Inner Ring and prevents its vertical displacement and rotation, closes the Spherical joint and serves as an interface with the rest of the MGSE or with a tripod.
Inner Ring	1	Contains the sphere and locks its position when force is applied on it by the External Case.
Sphere	1	Allows movement and pointing of the camera, provides connection with the cylindrical bracket.
External Case	1	Pushes the Inner Ring against the sphere to clamp it, and keeps all the inner parts in place.

Cylindrical Bracket	1	Provides a connection with the Support Plate and means to host the harness attached to the camera.
Camera Support	1	Serves as an interface with the Camera System.
ISO 4762 Screw M4x16 Hexagon Head Cap	1	Connect the Cylindrical bracket to the Camera Support.
ISO 4762 Screw M3x8 Hexagon Head Cap	2	Fix the External Case on the Bottom Plate.
ISO 4762 Screw M6x16 Hexagon Head Cap	1	It's used to clamp the External Case on the inner parts.

Table 13: Function explanation of each component.

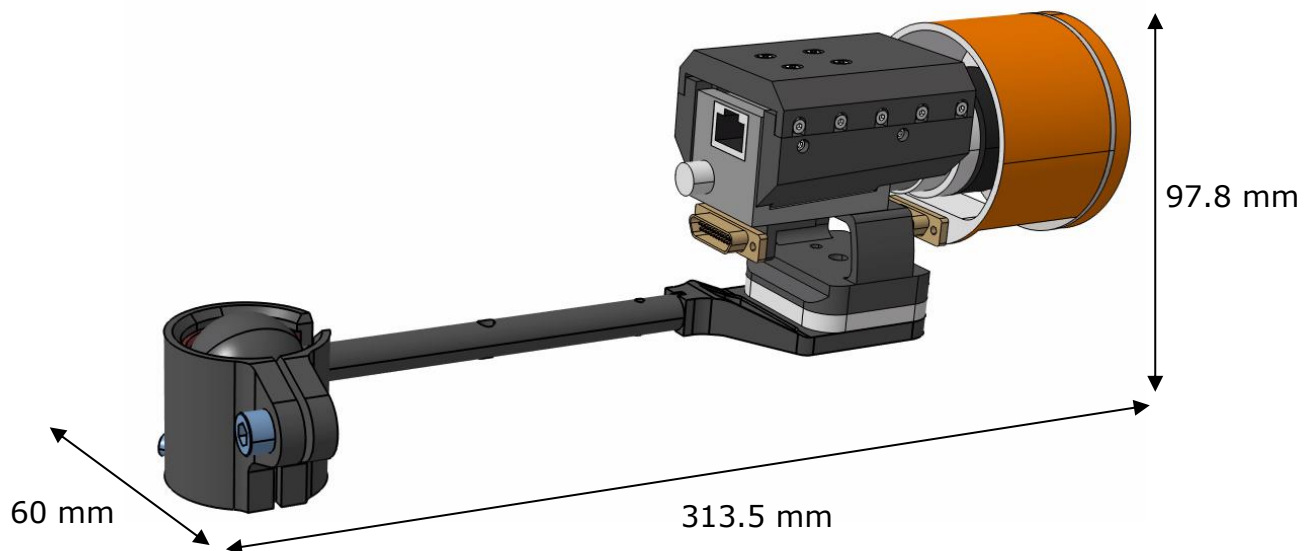


Figure 30: Spherical joint and support parts: overall dimensions.

Element	Material	Mass
Bottom Plate	Al 7075	0.021 Kg
Inner Ring	Vespel SP3	0.007 Kg
Sphere	Al 7075	0.036 Kg
External Case	Al 7075	0.045 Kg
Cylindrical Bracket	Al 6061	0.021 Kg
Camera Support	Al 6061	0.026 Kg
TOT		0.156 Kg

Table 14: Bill of Material and mass.

6.2 Components description

6.2.1 External Case

The external case has the function of keeping the joint in place and clamp the sphere. In order to do so, the upper part of the case is equipped with a shoulder, to prevent the vertical movement of the inner ring and the sphere, placed inside it. The two “ears” visible on the left in figure 31, both present a hole, one of them threaded (M6 1.5D helicoil), where a screw will be inserted and tightened to fix the ball. When tightened, the two ears will be pushed towards each other reducing the gap (nominally 2mm) and applying a force on the sphere via the inner ring.

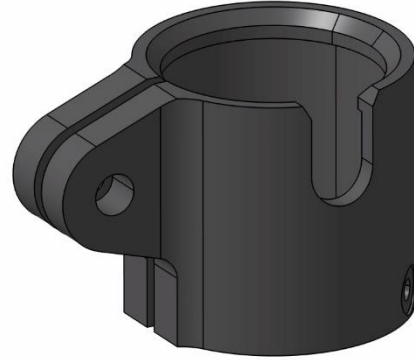


Figure 31: Eternal Case.

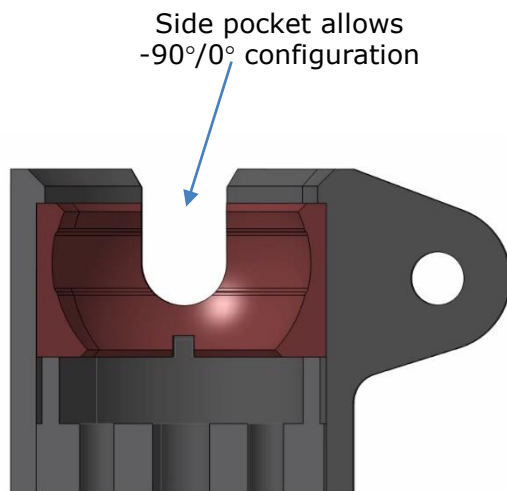


Figure 32: Spherical joint section.

The shape of the socket of the external case is designed so to achieve the desired pointing angles, which are:

- Elevation angle: $+90^{\circ}/-45^{\circ}$
- Azimuth angle: $\pm 15^{\circ}$

Moreover, rotation around the axis of the shaft is allowed, thus providing with the possibility of generating non-tilted images and orienting the camera in different ways (upside down for example, when horizontal configuration is used).

6.2.2 Bottom Plate

The bottom plate main purpose is to create a connection between the Spherical Joint and the MGSE or a tripod. To provide connection with the MGSE, 4 M4 2D helicoil threaded holes were designed, in order to confer a solid and stiff junction. A central imperial 1/4"-20 threaded hole was made to provide connection with standard



Figure 33: Bottom Plate.

tripods.

In a preliminary design, the bottom plate was fixed to the external case by thread, meaning the lower lateral surfaces of both parts were meant to be threaded around the 34mm diameter, with 1.5 pitch, in order to allow a small play between the parts, due to the thread itself. This was meant to allow the external case to have enough play to clamp the ball when tighten, by having the gap between the “ears” getting smaller. This solution was then discarded because of two main reasons: firstly, employing a threaded junction meant, in this context, introducing the threat of accidental unscrewing, violating the requirement FPR-1; secondly, manufacturing would be complicated.

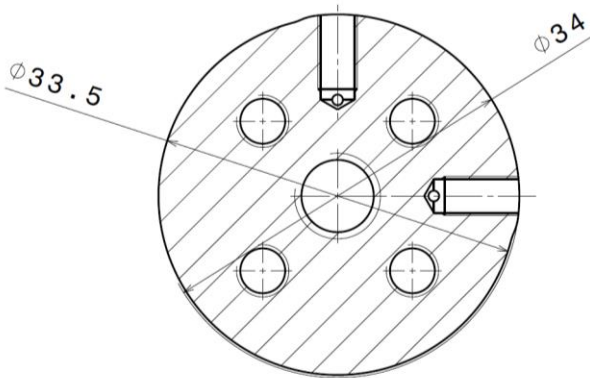


Figure 34: Bottom Plate Radii dimensions.

It was so decided to connect the two parts via two screws inserted in threaded holes on the side of the component, visible in picture 33, placed 90° apart from each other, on the opposite side of the cut and the bolt in the external case. In order to have play between the parts and allow the external case to clamp the sphere, a 90° sector of the bottom plate, where the holes are places, has a diameter of 34mm (tolerances will be discussed in section 7.3) while on the remaining 270° the diameter is 33.5mm, as shown in figure 34.

As regards the upper part of the bottom plate, a circular shoulder was designed to prevent vertical motion of the inner ring, while the two smaller shoulders positioned 180° from one another, are meant to prevent its rotation.

6.2.3 Sphere

The ball has very simple design, the flat surface on the top was made to allow easier machining and to simplify the mounting of the cylindrical bracket, connected to the threaded hole on the top.

In an early concept design, the sphere and the cylindrical bracket were meant to be a single part, but as explained in section 5.2, two different brackets were created in order to allow different applications. For this reason, the sphere and the bracket needed to be separated and connected in a way to allow mounting and separating them several times.



Figure 35: Sphere.

6.2.4 Inner ring

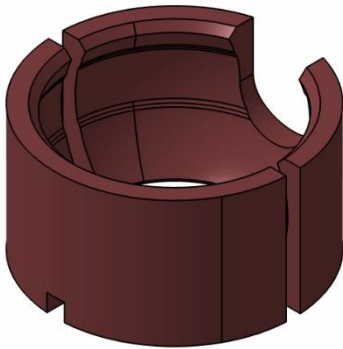


Figure 36: Inner Ring.

The inner ring is positioned around the sphere and is divided into two parts for mounting purposes. As shown in figure 36, the outer part is shaped a cylinder and it's in contact with the inner walls of the external case, while the inner is shaped as a sphere to maximise the contact with the ball. In the internal part a spherical groove of 0.2mm is carved all around the piece. That is to avoid point contact once the inner ring is pushed again the sphere when they're clamped together.

The two cuts place 180° from one another, are made to host the bottom plate's small shoulders, as previously discussed in section 7.2.1

6.2.5 Cylindrical bracket (version A)

The cylindrical bracket connects the spherical joint to the camera support plate.

The connection with the Spherical Joint is exploited via a threaded pin (visible on the left in figure 37) that is part of the component and will be inserted in the sphere (M6 helicoil).

On the other end of the Bracket, a M4 threaded hole was designed, that will serve as a connection with the Camera support, via a screw. Two small pins are made to be inserted in the support camera, in order to prevent the unscrewing of the bolt and avoid rotation.



Figure 37: Cylindrical Bracket.

In the middle of the cylinder there is a small hole with the purpose of facilitating the tightening on the bracket on the sphere.

The cylindrical shaft that supports the camera system must be sufficiently long for two reasons:

1. To leave enough space for the harness of the camera
2. So that the field of view of the camera is not obstructed when in horizontal configuration

Point 1 translates into a minimum length for the shaft of 10 cm, which accounts for the space needed not to damage the cables.

Point 2 needs some geometrical considerations:

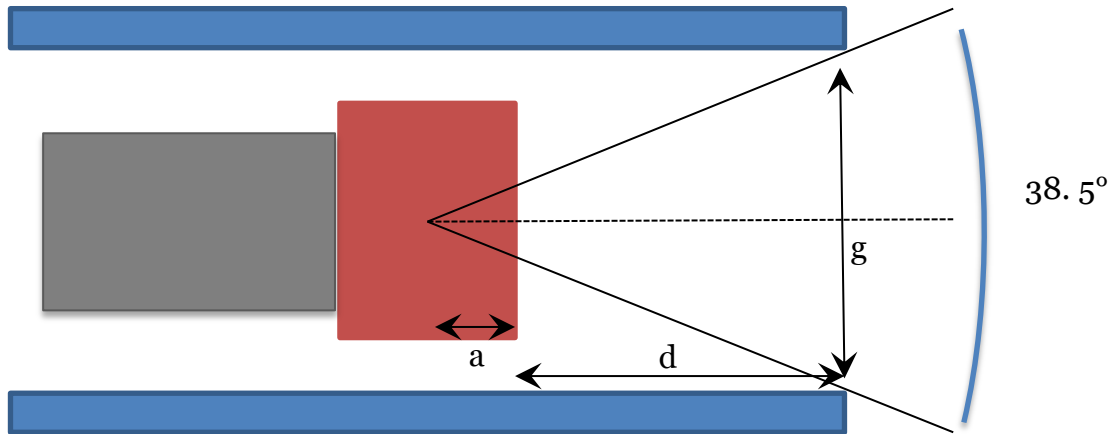


Figure 38: FoV of the camera.

Description	
Angle FOV	38.5°
Gap between lateral brackets (g)	74 mm
Distance between focus and camera front (a)	22.80 mm
Resulting maximum distance (d)	57.41 mm

In order to meet point 1 shaft length is set to 10 cm (intended as the length of the cylindrical part starting from the surface of the sphere). It follows a distance d of 42.92 mm, which is below the maximum derived from point 2.

6.2.6 Camera Support

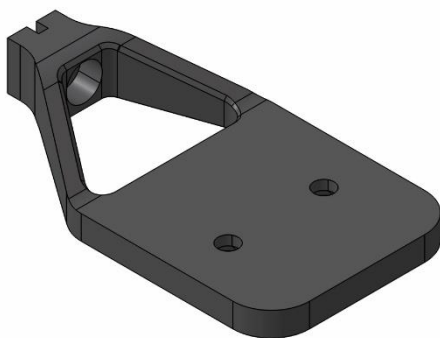


Figure 39: Camera Support.

This component represents the interface between the spherical joint and the camera system. The dimensions of the plate match the camera's one, in order to best accommodate it. The section that connects it with the cylindrical bracket is higher to allow the insertion of the screw.

The 2 mm pocket, visible in the top left in figure 39, is made to accommodate the shoulders of the cylindrical bracket and prevent its rotation.

Also, two holes were created in the plate to allow the connection with the camera system via the insertion of bolts.

It's necessary to point out that, even if not discussed in each section, in all the previous components, for every blind hole (for example the 2 threaded holes on the side of the

Bottom Plate), a ventilation hole was created in order to let the air flow out and avoid air pockets that could damage the parts once inserted in vacuum environment.

If the air cannot flow out of the holes once vacuum is made, the pressure on the inside of the holes would be higher and could destroy or severely damage the components, or leak during the test contaminating the test environment.

6.3 Installation process and tolerances

The process to be followed for the installation and preparation of the Spherical joint is shown in Figures 40 to 43:

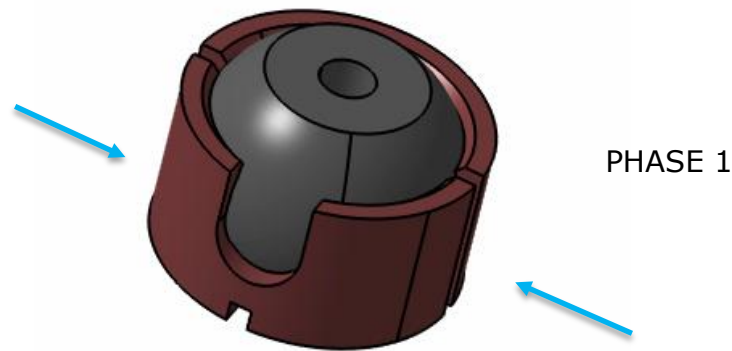


Figure 40: Installation, phase 1: insertion of the Inner Ring on the Sphere.



Figure 41: Installation, phase 2, 3 and 4: Completion of the Spherical Joint.



Figure 42: Installation, phase 5: Connection with the Camera Support.

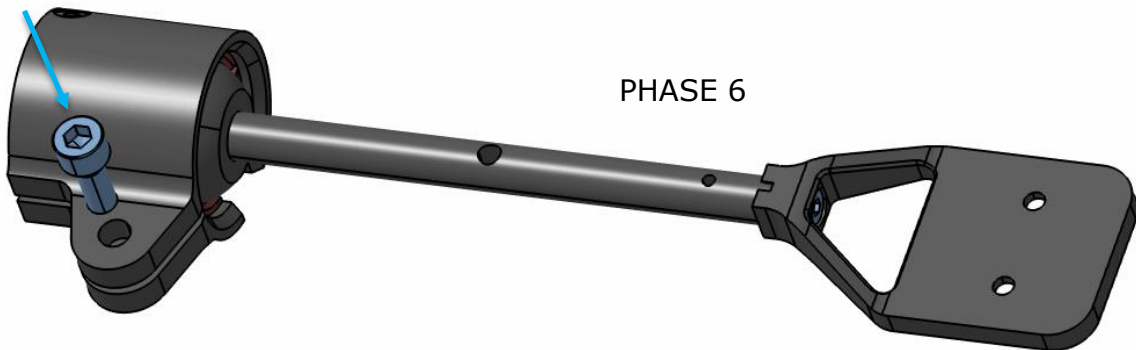


Figure 43: Installation, phase 6: Fixing of the position.

Tolerances were defined for all the parts that are coupled. The tolerances have to be wide enough to be able to generate a big enough gap and to allow the manufacturing but narrow enough to allow the clamping of the sphere without generating excessive stresses on the components. The nominal dimensions of the coupling can be seen in figure 44.

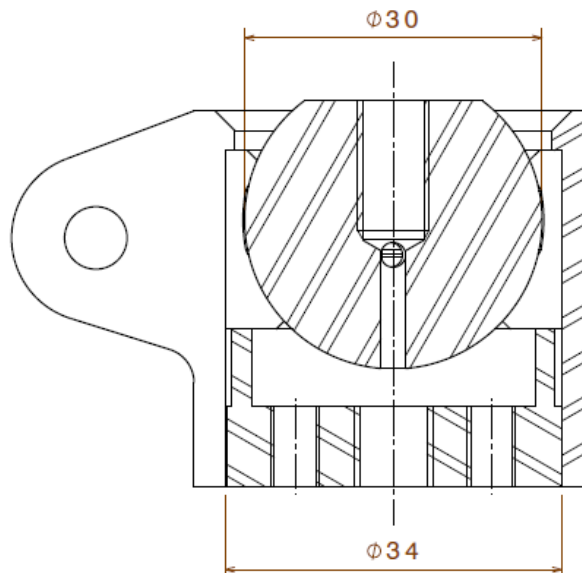


Figure 44: Nominal dimensions.

Component	Nominal dimension	Tolerances
Sphere	30mm	+/- 20 microns
Inner Ring (inside diameter)	30 mm	+/- 30 microns
Inner Ring (outside diameter)	34 mm	-70/-100 microns
External Case (inside diameter)	34 mm	+/- 20 microns

Table 15: Tolerances.

This combination of tolerances allows, in case all the parts have the maximum measure to generate play, to have a total gap of 170 microns and, in the opposite case, a minimum gap of 0 microns, with which the components will still be able to be mounted inserting the eternal case in an oven, and the sphere in a fridge before mounting them, to take advantage of the thermal deformation and create enough play to allow the mounting.

Component	Nominal dimension	Play	Interference
Sphere	30mm	-20 microns	+20 microns
Inner Ring (inside diameter)	30 mm	+30 microns	-30 microns
Inner Ring (outside diameter)	34 mm	-100 microns	-70 microns
External Case (inside diameter)	34 mm	+20 microns	-20 microns
Maximum Play	170 microns		
Maximum Interference	0 microns		

Table 16: Maximum and minimum play for the spherical joint.

In order to define the definitive value of the torque to be exert on the bolt to clamp the sphere, it is necessary to take into account the results of the preliminary calculation. In section 5.3, thermal analysis, it was calculated that when the chamber reaches cryogenic temperatures, an overall play of 23 μm is generated.

Considering the higher possible gap generated by the tolerances, 170 microns, and the 23 μm in cryogenic conditions, a total gap of 193 μm will have to be compensated.

In order to calculate the torque to apply to the bolt to close the gap, a quick static FEM (Finite Elements Method) analysis was run on the External Case through CatiaV5. To do so, the part was modified as shown in figure 45.

To better simulate the connection with the bottom plate, a 105° angular pad was created, on the same section where the bottom plate has the diameter of 34mm and the two parts are in contact, hence where the external case is fixed.



Figure 45: External Case for analysis

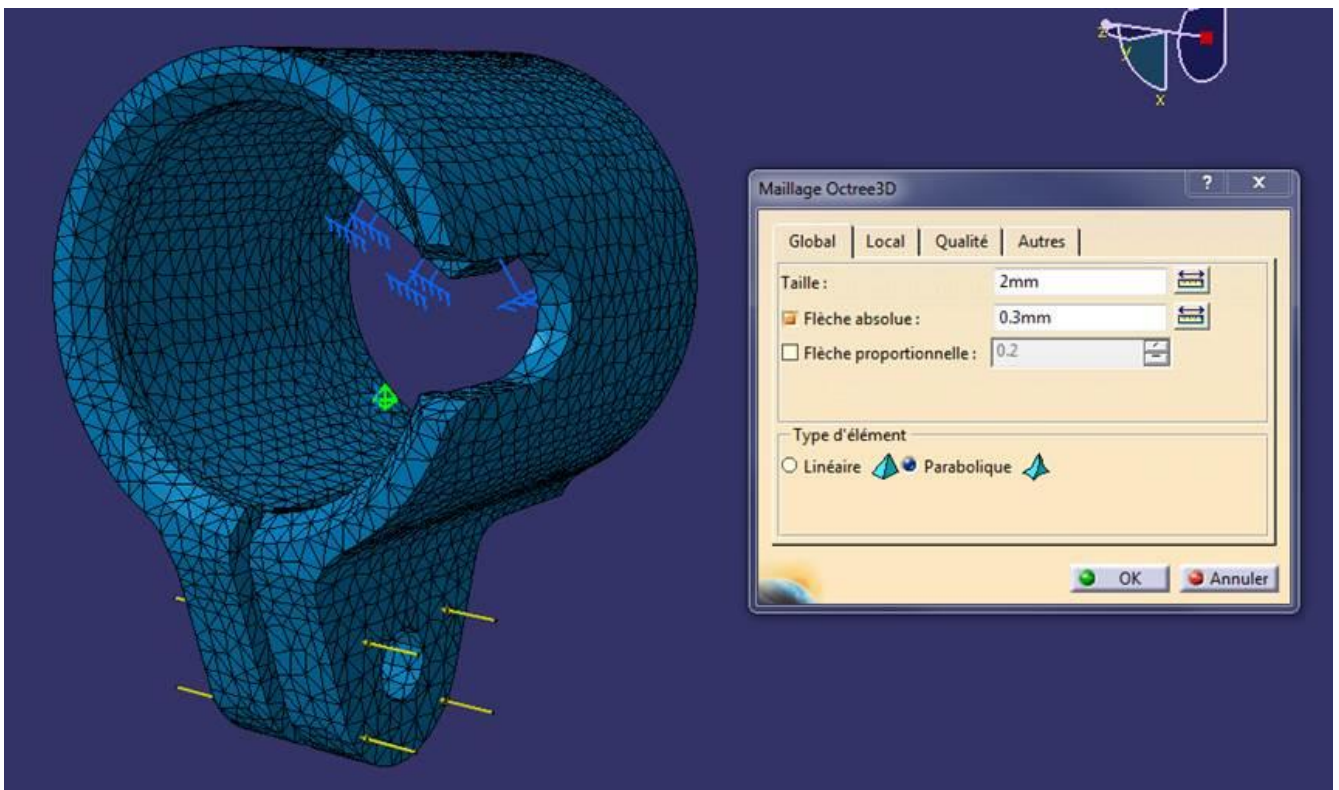


Figure 46: Display of mesh settings.

CATIA V5 generates an automatic mesh, meaning that nodes are not manually defined. However, parameters such as mesh size, absolute sag and type of mesh are user-definable.

As displayed in figure 46, a parabolic type of element was chosen, since this element type is automatically created with intermediate nodes, it is better suited to mesh a part where most of the surface is curved, such as the external case. Employing a linear element type would mean having to sensibly reduce the mesh size to achieve a similar level of accuracy.

As for the other parameters, an element size of 2mm as well as a sag size of 0.3mm, were considered optimal for this analysis, given the total dimensions of the piece.

As regards the constraints, they are displayed in figure 47. A clamp constraint was created on the lateral surface of the angular pad, to simulate the bolted connection with the bottom plate. The load was applied on the external surfaces of the “ears”, to push them together in the same way the bolt would, once inserted to clamp the joint.

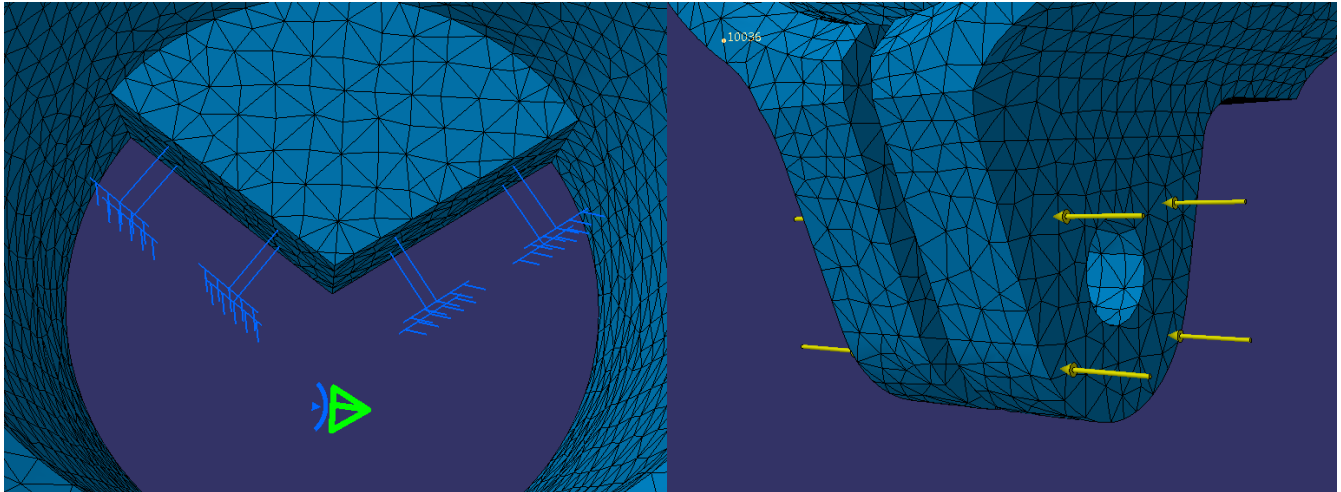


Figure 47: constraints and load.

A simulation was run applying a 1N force on the clamping bolt, (0.5N on each side) in order to evaluate radial displacement of the internal diameter, per Newton:

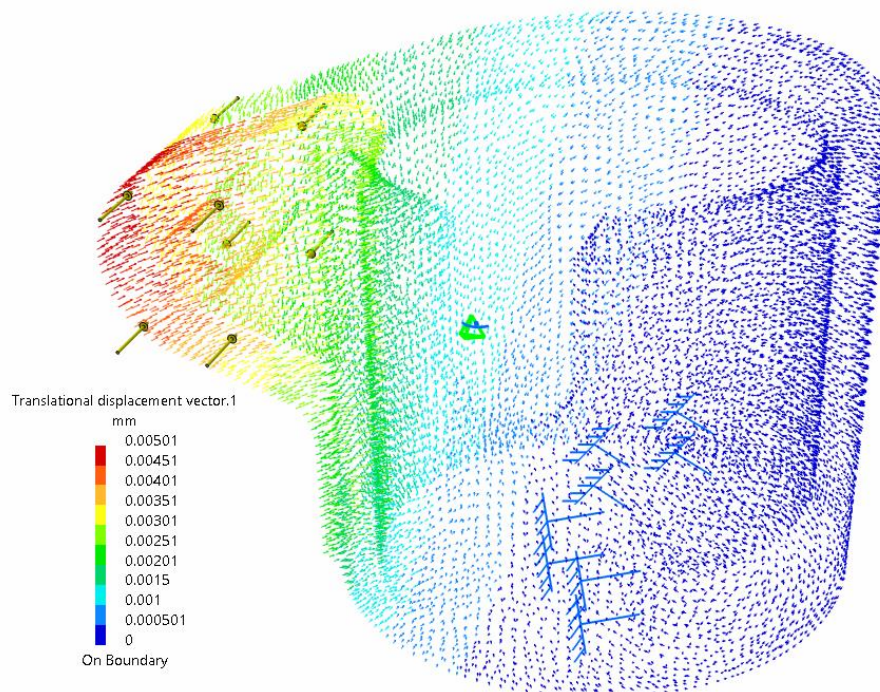


Figure 48: Translation displacement of External Case under 1N load.

As shown in figure 46, when the load of 1N is applied, the radial displacement is 0.0015 mm, 1.5 microns. The displacement per unit of Newton is $1.5 \frac{\mu\text{m}}{\text{N}}$, in order to close the gap between the External Case and the Sphere, the load to be applied is:

$$F_G = \frac{193 \mu\text{m}}{1.5 \frac{\mu\text{m}}{\text{N}}} = 128.6 \text{ N}$$

The total clamping force is obtained adding this value to the preliminary clamping force calculated in section 5.2:

$$F_B = 167 \text{ N}$$

$$F_T = 167 \text{ N} + 128.6 \text{ N} = 295.6 \text{ N}$$

$$M_B = fDF_B = 0.2 \times 6 \times 10^{-3} \text{ m} \times 295.6 \text{ N} = 0.35 \text{ Nm}$$

Hence the torque to be applied on the bolt is 0.35 Nm or higher.

7 MANUFACTURING AND TEST

7.1 Test Procedure

Initially, one spherical joint has been manufactured and built as a prototype, in order to validate and test the design.

Due to the delay in the delivery of the material, the prototype of the inner ring, in VespelSP3, was manufactured in out of a rod of 25mm, for this reason the prototype of this part is divided in four parts instead of two.

As regards the rest of the parts, they have been manufactured and sent to be anodized to an external company.

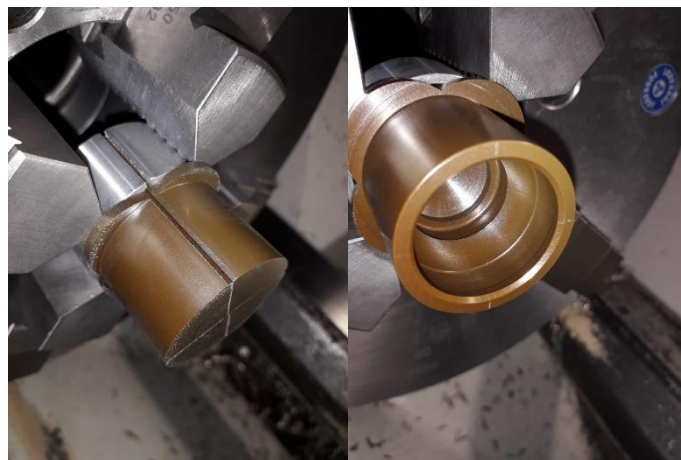


Figure 49: Manufacturing of inner ring.



Figure 50: Manufactured parts: before and after anodization.

To validate the component, a test procedure was drafted to evaluate the behaviour of the spherical joint in vacuum at cryogenic temperatures. For this purpose, LIVAF (Little Vacuum Facility), a small cryogenic-vacuum chamber was selected for the test. This chamber is also equipped with a window on the door, which allows to monitor the test.



Figure 51: LIVAF.

To exploit the test, new parts were designed to provide support and connect the spherical joint with the test facility. In figure 48, the general test set up in shown.

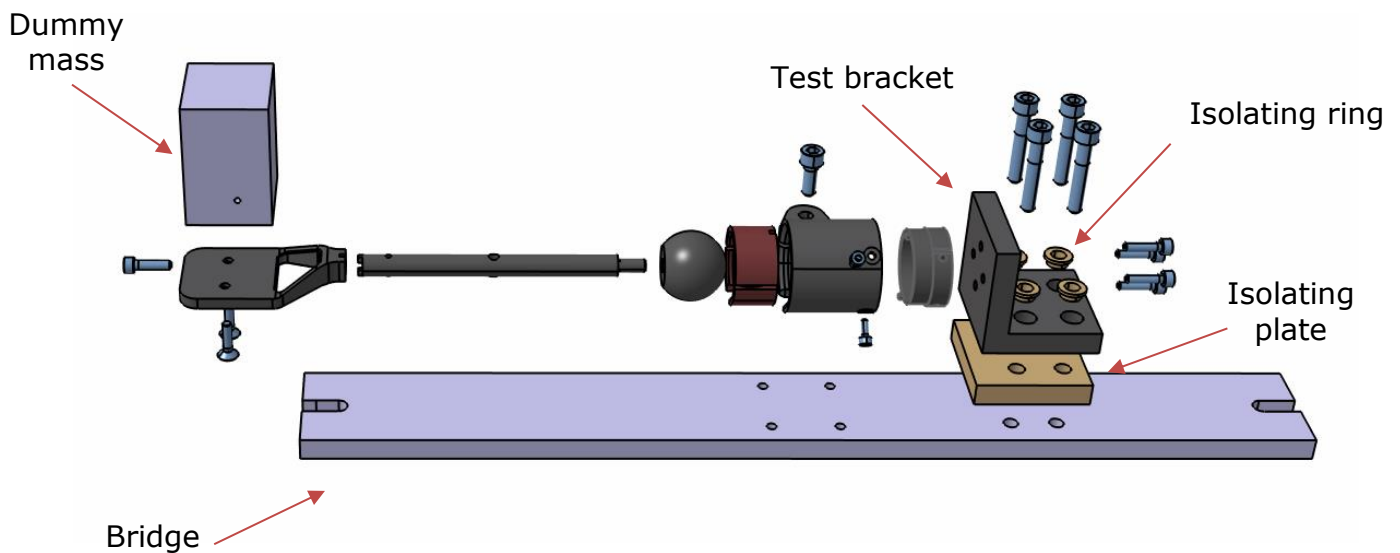


Figure 52: test set up.

Element	Quantity	Material	Function
Bridge	1	Al 6061	Represents the connection with the chamber, the extremes are in contact with the shrouds and fixed to the them by means of screws.
Isolating Plate	1	PEEK	Thermally decouples the Spherical Joint from the shrouds.
Isolating Ring	4	PEEK	Insert to avoid the appearance of thermal paths through the screws.
Test Bracket	1	Al7075	Serves as a connection between the spherical joint and the bridge, to allow the installation of the spherical joint in a fixed position.
Dummy Mass	1	Stainless Steel	For testing purposes, a dummy mass is placed on the Camera Support. A Safety coefficient of 2 was employed, hence the mass is 826g, twice the one of the Camera System.
ISO 4762 Screw M4x16 Hexagon Head Cap	4	Stainless Steel	Connects the Cylindrical bracket to Camera Support.
ISO 10642 Screw M4x16 Hexagon Countersunk Head	2	Stainless Steel	Fix the Dummy mass on the Camera Support.
ISO 4762 Screw M6x35 Hexagon Head Cap	4	Stainless Steel	Connect the Test Bracket to the Spherical Joint via the Bottom Plate.

Table 17: Function explanation of each component and BoM.

The isolating plate and rings were designed in order to avoid the appearance of thermal paths and decouple the Spherical Joint from the shrouds. The rings are inserted between the bolts and the test bracket, while the plate is mounted between the bridge and the test bracket, avoiding conduction, as shown in figure 49.

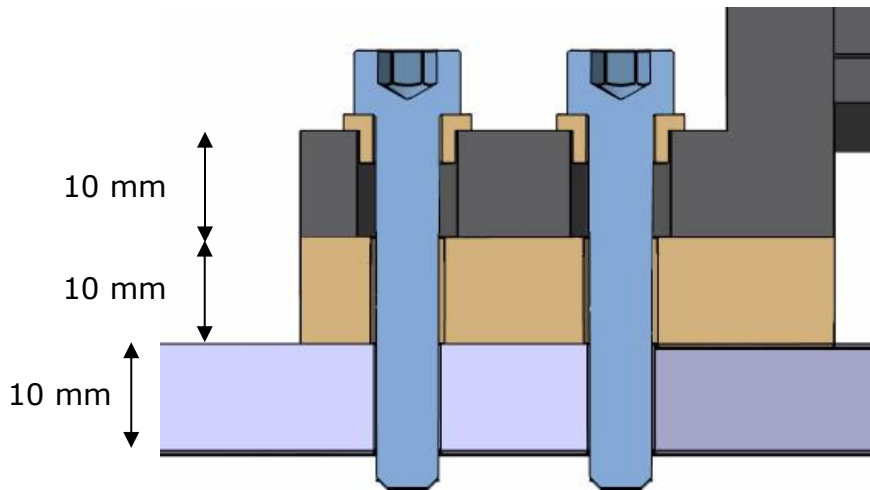


Figure 53: Insulator section.

Before inserting the component in the thermal vacuum chamber, a quick test in ambient was carried out.

In order to investigate the movement of the ball head, a small ruler is installed attached to the bridge and a camera with a tripod is positioned in front of the chamber window and kept in the same position throughout the test.

The component was tightened with 0.5 Nm torque, which required 135° rotation of the M6 bolt, pictures were taken 24 hours apart from each other, to check if the ball would slide or not in this timeframe.

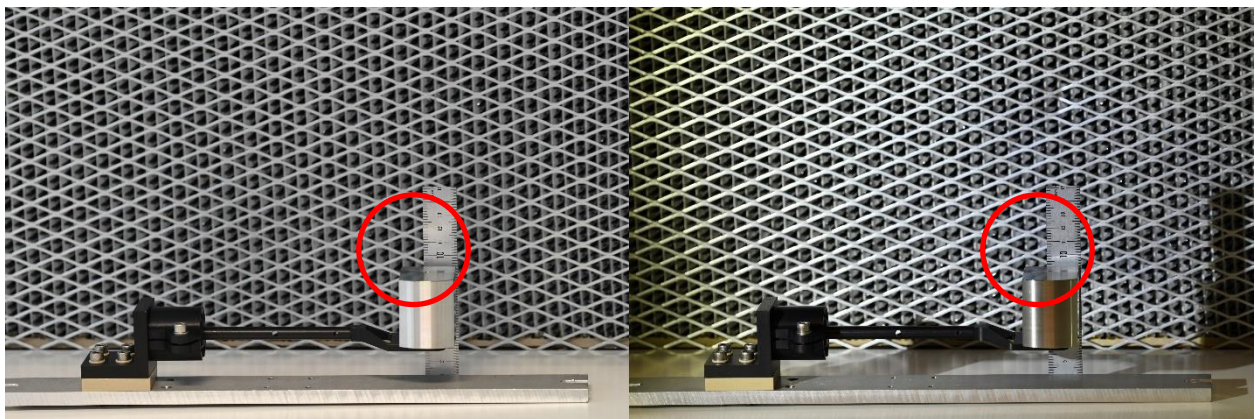


Figure 54: Test in ambient atmosphere: on the left the component at the beginning of the test, on the right the component 24 hours later.

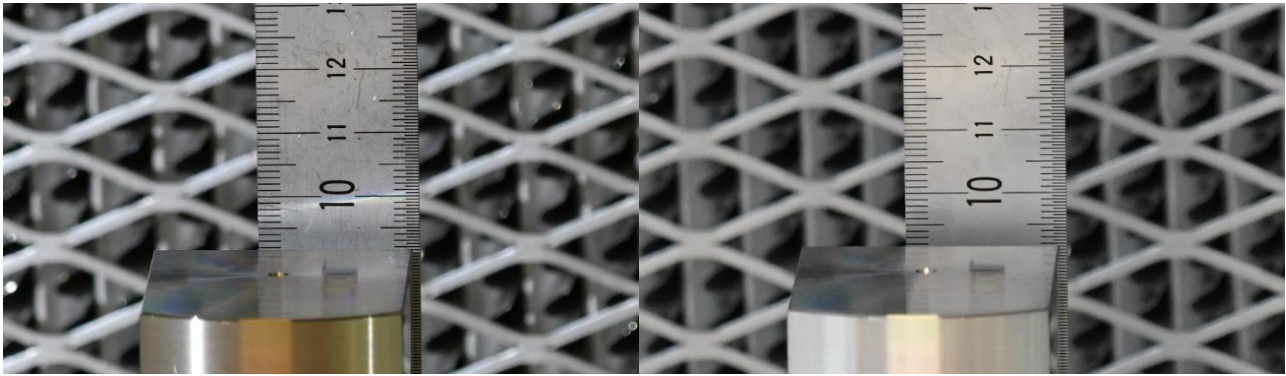


Figure 55: Close up of figure 52.

As shown in figures 52 and 53, the spherical joint remained fixed in the initial position and did not show any signs of movement. Once this procedure is completed, the component is considered ready to be tested in the thermal vacuum chamber.

The temperature is monitored, throughout the test, via 8 thermocouples that equip the component, in the following positions:

Thermocouple	Position
1	Shroud
2 and 3	Bridge: one on the side (close to the shrouds) – one in the middle
4	Test bracket
5 and 6	External Case: one on each side
7 and 8	Cylindrical Bracket: one on each side

Table 18: Thermocouples position.

The greatest temperature gradients are expected between 2-3 and 4 and between 5-6 and 7-8, since in those areas the metallic parts are separated by plastic components.

The thermocouple of reference to control the test are 5, 6, 7, and 8, since they measure the temperature around the spherical joint.



Figure 56: Installation of thermocouples and display of the camera set up.

The testing procedure is drafted to qualify the component for vacuum, cryogenic applications. Details of the test are presented in table 19.

Number of Cycles:	4.
Temperature:	LN2. (-180 °C)
Stability:	2K/h.
Dwell Time:	2 hours.
Pressure:	Below 10e-5 mbar.

Table 19: Test Details.

7.2 Test Description and Results

Figure 55 shows the four temperature cycles, labelled in the red rounds, which the specimen underwent during the test.

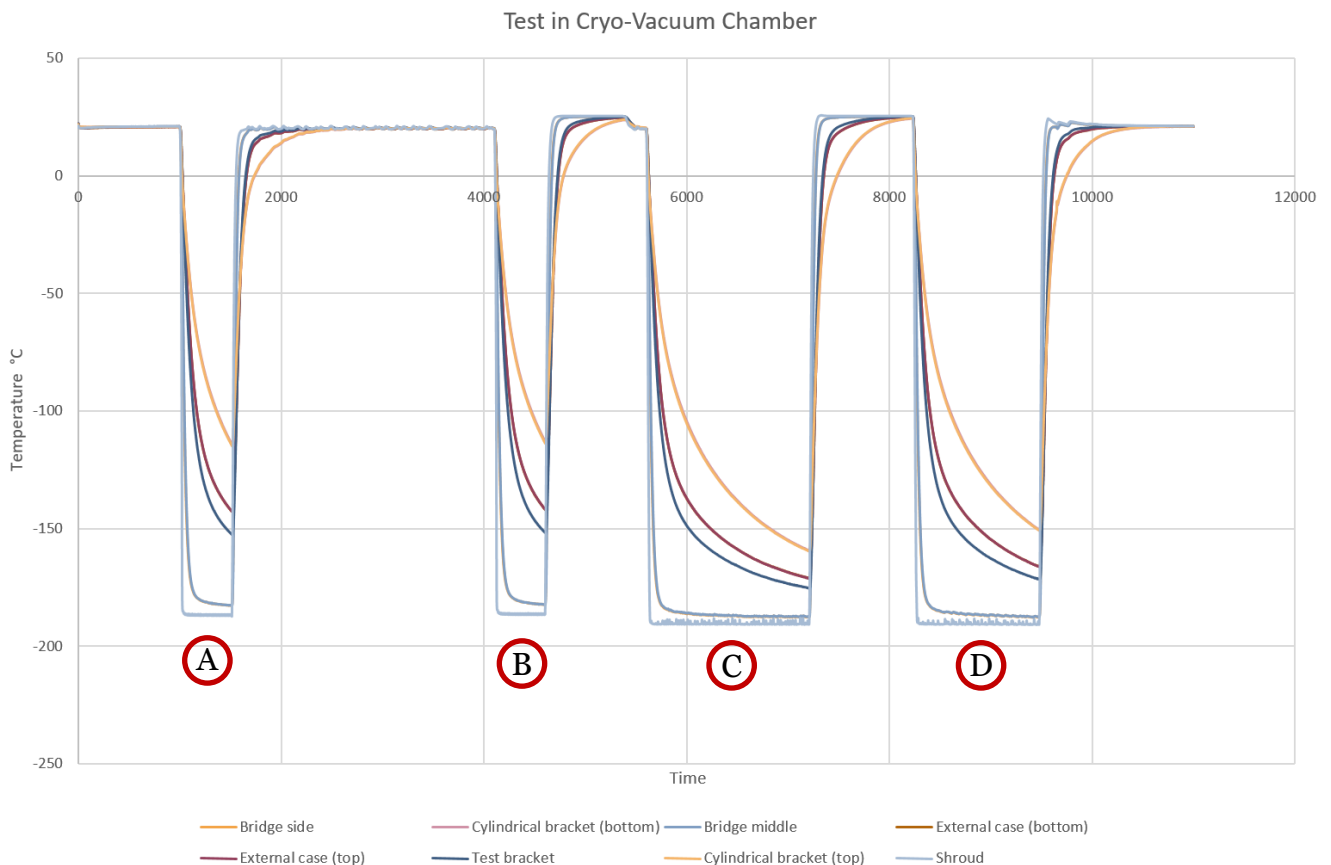


Figure 57: Test temperature cycles.

Throughout the test, several measurement pictures were taken in order to monitor the behaviour of the spherical joint. Figure 56 shows the temperature cycles again, indicating the temperature and times at which the most relevant measurements were made.

Test in Cryo-Vacuum Chamber

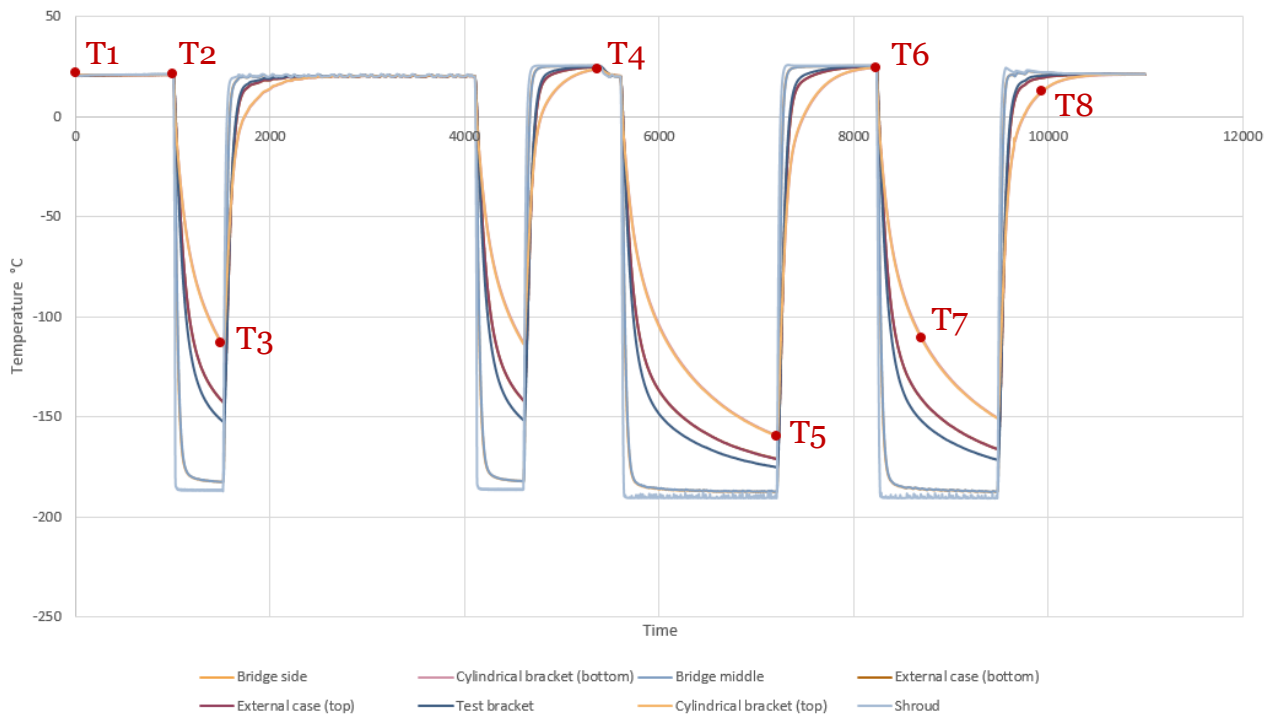


Figure 58: Measurement points graph.

Point	Time [minutes] (Since the start of the test)	Temperature [°C] (Cylindrical Bracket Top)
T1	0	21.9
T2	996	21
T3	1491	-112.9
T4	5363	23.8
T5	7203	-159.5
T6	8224	24.5
T7	8693	-110.7
T8	9938	12.6

Table 20: Measurement points table.

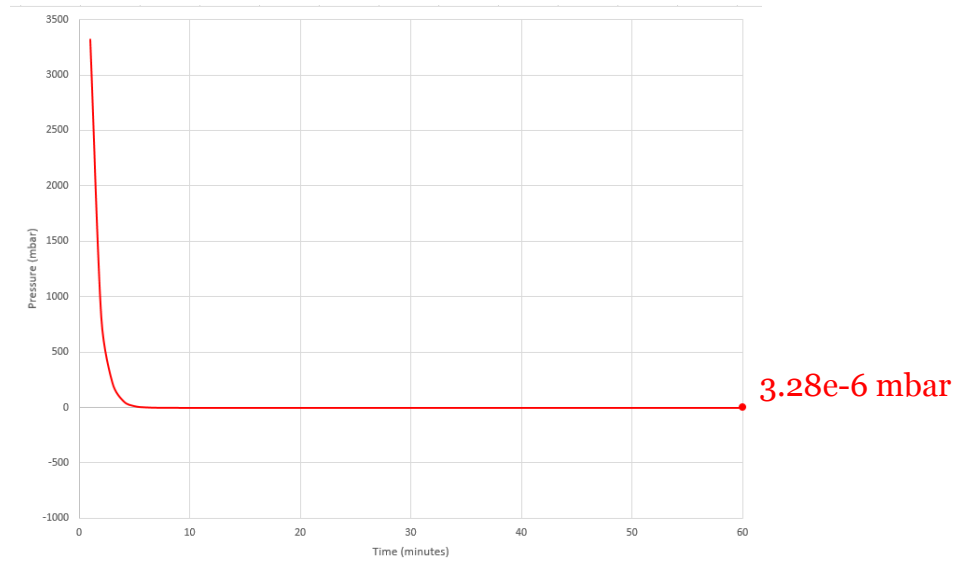


Figure 59: Pressure drop during the first hour of the test.

As shown in figure 57, within the first hour since the beginning of the test, the pressure reached $7.47e-5$ mbar, but the cooling down began when it reached $3.28e-6$ mbar, 15 hours later.

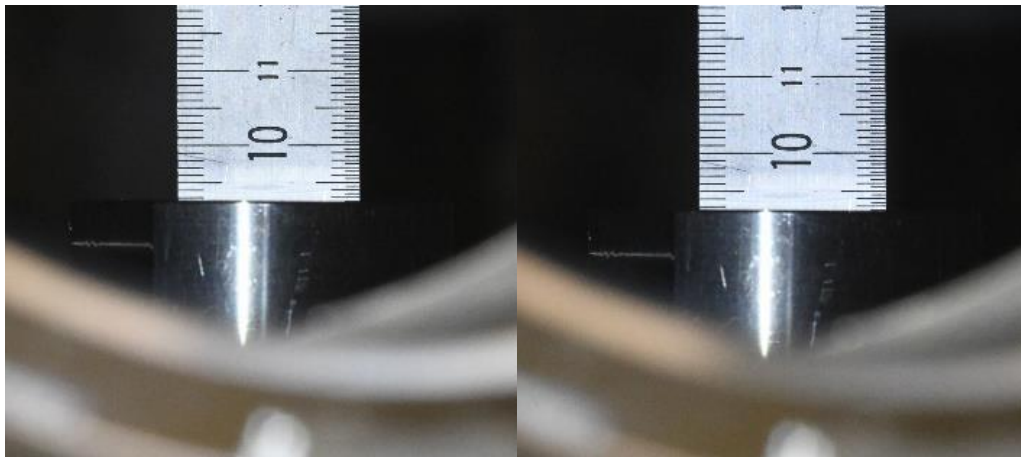


Figure 60: On the left, Spherical joint in ambient temperature and atmosphere. T1
On the right, Spherical joint in ambient temperature and vacuum ($3.28e-6$ mbar). T2

Figure 58 shows the spherical joint setup right before the beginning of the first cycle, in ambient temperature and atmosphere on the left, and ambient temperature and vacuum on the right. Comparing the left and right pictures, it is visible that the ball head remains fixed in the original position when the pressure inside the chamber is dropped.

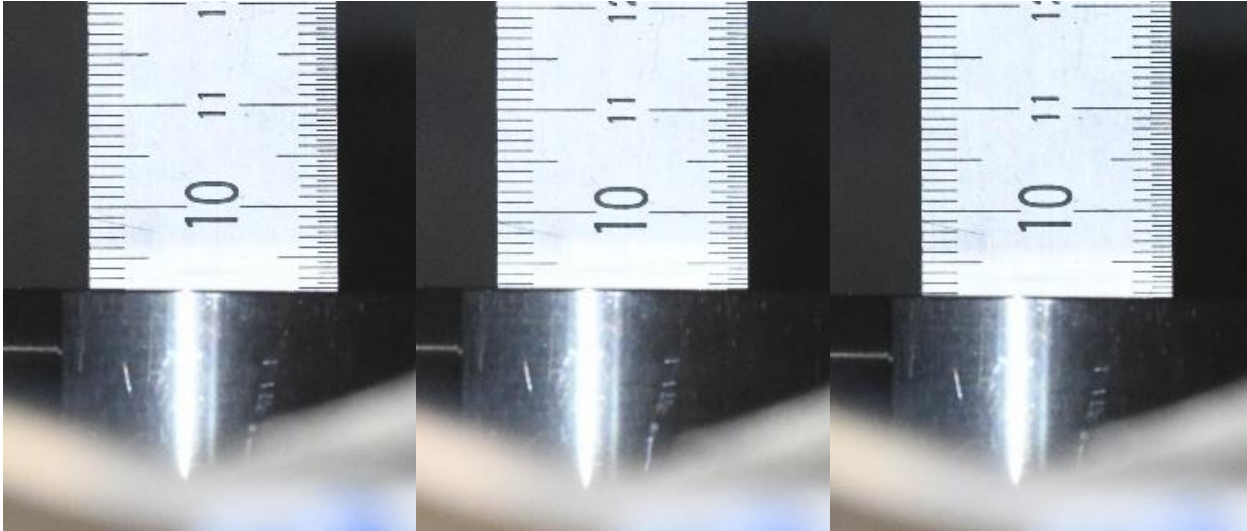


Figure 61: Points T3, T4 and T5 (from left to right).

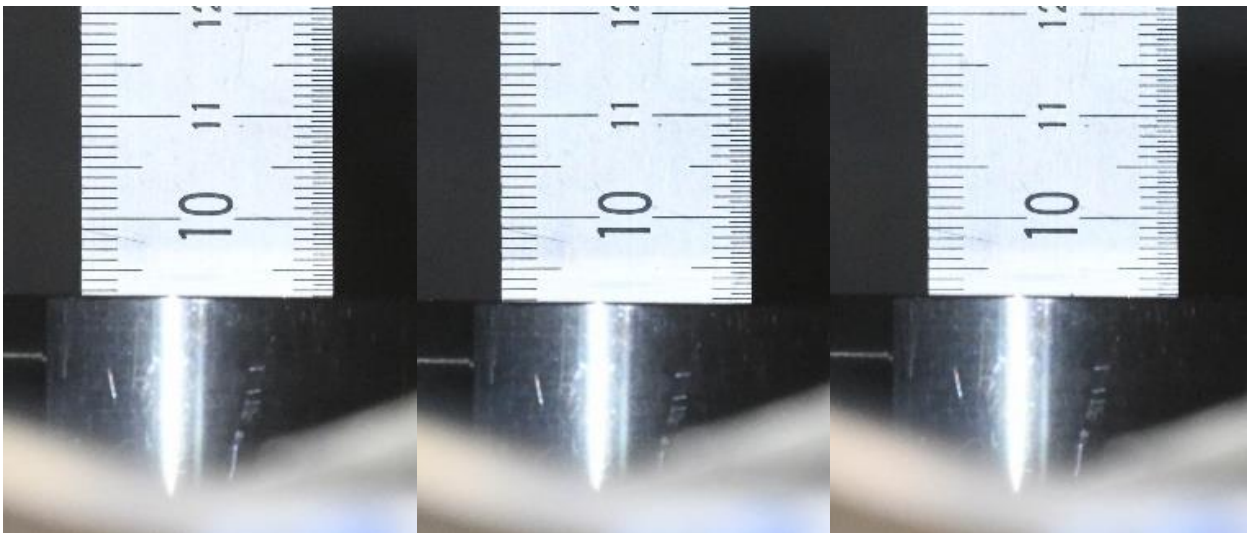


Figure 62: Points T6, T7 and T8 (from left to right).

Figures 59 and 60 show the measurements for the points T3 to T8. Comparing these measurements, it is visible that the dummy mass is in a different position, about half a millimetre lower, when the component reaches the lower temperature of the cycles. However, at the end of every cycle, when the temperature reaches 20 degrees, the position is once again the original one. This clearly shows that the movement is not due to the sphere sliding against the inner ring, but to the thermo-elastic deformations of the parts, inevitable with the temperature drop.

After the end of the test the component was dismantled and all the parts resulted to have preserved the original shape and integrity, hence Spherical joint prototype is considered qualified for Vacuum chambers applications.

8 CONCLUSIONS

The purpose of this paper is to explain the process of the realization of a MGSE for the new photogrammetry system that has been developed at the ESTEC Test Centre. This hardware, employed to measure the thermo-elastic deformations, has been recently successfully qualified for thermal vacuum operations. The eight cameras must be used in several thermal vacuum chambers, at ESTEC but not limited to. The MGSE most crucial component is the spherical joint, that will need to be still and fixed once inserted in the thermal vacuum chamber, in order to allow the test; but able to move and allow a change on the field of view of the camera once the test is completed, for several cycles of testing. For these reasons, the greater part of the paper focuses on the conception, design and testing of the parts that make up the spherical joint. The ball-head was not only designed but also manufactured and tested in a small vacuum chamber to qualify the product.

Initially, a broad bibliographical research was carried out, concerning especially the choice of materials to use in such high friction-vacuum-cryogenic application, which proved itself to be unusual. Once the materials have been selected, a design was made by means of CATIA V5, and FEM analysis were run to ensure the consistency of performances, conducting an iterative process to obtain a prototype design ready to be manufactured and tested. The main requirements that lead the design are the necessity of having a small, light, easy to install tool, while minimizing maintenance activities and the capability of having consistent performances both in ambient and in cryogenic-vacuum environment (the MGSE has to operate under the following conditions: Temperature: 100 to 313 K, Relative Humidity: 40% to 60%, Pressure: $3e-7$ mbar), taking into account the tribological aspects throughout in the process.

The main difficulties lied in: the use of different materials, that had to be coupled to ensure the consistency of performances in vacuum chambers, while tolerances must not be excessively tight, in order to allow the mounting and dismounting of the assembly; the limited researches available on tribology for such high friction vacuum application, and on the difficulty of modelling the physical constraints in FEM analysis on CATIA V5. These difficulties have been faced by applying security factors and by means of a continuous bibliographical research.

An extensive explanation of the design and test support was carried out in chapter 6, in order to justify the conceptual choices that were made in the process. In chapter 7, a description of the test was carried out, the results prove the design to be consistent and qualify the component for thermal vacuum chambers applications.

Future works include the supervision of the manufacturing and mounting of the 8 ball-heads, as well as the preparation and finalisation of the design and the manufacturing of the remaining parts of the MGSE that haven't been discussed in detail in this paper.

9 DEFINITIONS AND ABBREVIATIONS

MGSE	Mechanical Ground Support Equipment
TV	Thermal Vacuum
LSS	Large Space Simulator
ESA	European Space Agency
ESTEC	European Space Research and Technology Centre
TB/TV	Thermal Vacuum and Thermal Balance
TEC-MXE	Directorate of Technology, Engineering and Quality; Test Centre Division; Engineering Services Section
COTS	Commercial off the shelf
HSCS	High Speed Camera System
LEAF	Large European Acoustic Facility
HYDRA	Multi-axis Hydraulic Vibration Facility
MAXWELL	Large Electromagnetic Compatibility Facility
CPS	Central Pumping System
HVP	High Vacuum Pumping system
SNSE	Shroud and Nitrogen Supply Equipment
LN ₂	Liquid Nitrogen
GN ₂	Gaseous Nitrogen
CVD	Chemical Vapor Deposition
PVD	Physical Vapor Deposition
FPR	Functional and Performance Requirements
IR	Interface Requirements
ER	Environmental Requirements
DR	Design Requirements
FEM	Finite Elements Method

10 BIBLIOGRAPHY

- R1 ESR Technology Ltd. (2013). *Space Tribology Handbook* .
- R2 Anderson M J, B. M. (2010). *Hard, High Friction Interfaces for Space Applications*.
- R3 Andreson M J. (1994). *The Friction and Wear of Polymeric Materials at Cryogenic Temperatures in Vacuum*. ESTL-TM-143.
- R4 Asadurian A., P. R. (2004). *A strain-free lock and release mechanism for an elastically suspended two-axis gimbal*. Proc 37th Aerospace Mechanisms Symposium, NASA/CP-2004-212073.
- R5 Bai Q. (2014). *Interactions between Wear Mechanisms in a WC-CO / Ti-6Al-4V Machining Tribosystem*.
- R6 Boesiger Edward A. (2004). *37th Aerospace Mechanisms Symposium*.
- R7 Boesiger Edward A., L. E. (1999). *33rd Aerospace Mechanisms Symposium*.
- R8 Buttery M, C. M. (s.d.). *Recent Observations on the Performance of Hybrid Ceramic Tribocontacts* .
- R9 Chaput D. (1994). *Payload Hold-down and Release Mechanism*. Proc 28th Aerospace Mechanisms Symposium, NASA CP-3260.
- R10 Durand M. (2003). *Plane/plane contact: Selection of material pairs with high friction*. Proc 6th ESMATS, ESA SP-480.
- R11 ESA Requirements and Standards Division . (2019). *Space Engineering Mechanisms*.
- R12 Gill S., R. R. (1992). *Static Adhesion in Preload Contacts subjected to Long-term Vacuum Exposure*.
- R13 Gniewerk J, C. R. (May 1961). *Thermal Expansion of Technical Solids at Low Temperatures* . Washington: National Bureau of Standards.
- R14 Gould, S. (1987). *The Friction and Wear of Materials at Very Low Temperature*. Risley, England.
- R15 Haslehurst A. (2003). *Clamp Band Assembly for the Beagle 2 Lander*. Proc 10th ESMATS, ESA SP-524.
- R16 Holzbauer R., J. C. (2015). *Evaluation of cold welding of stainless steels and Ti-6Al-4V in launch conditions* .
- R17 Holzbauer R., M. A. (2015). *Cold Welding in Launch*.
- R18 Joscelyn E, C. R. (1998). *Deployment of a Large Rotating Positioning System*. Proc 32nd Aerospace Mechanisms Symposium, NASA/CP-1998-207191.
- R19 K, P. (1984). *The Importance of Thermal Vacuum Testing in Achieving High Reliability of Spacraft Mechanisms*.
- R20 Kamarruddin K, A. S. (2017). *Performance Evaluation of Palm-Olein TMP Ester Containing Hexagonal Boron Nitride and an Oil Miscible Ionic Liquid as Bio-Based Metalworking Fluids*. Faculty of Mechanical Engineering, Universiti Teknologi Malaysia.
- R21 Lewis Simon D., R. R. (1997). *Hybrid Polymeric Bearings for Space Applications*. Warrington, UK.

- R22 Merstallinger A. (2005). *Contact adhesion and its prevention*. Lucerne: Space Tribology Course.
- R23 Nitschko T., F. M.-V. (1999). *The XMM Deployment Mechanisms: Mirror Doors and Sun Shield*. Proc 33rd Aerospace.
- R24 Privat M., D. C. (2003). *Pneumatic locking device for magnetic bearing reaction wheel*. Proc 10th ESMATS, ESA SP-524.
- R25 Qunitana F, E. J. (2003). *Preloaded launch locking devices for heavy equipment*. Proc 9th ESMATS, ESA SP-480.
- R26 Roberts D. (1987). *The Friction and Waer of Materials at Very Low Temperature*.
- R27 Roberts E W. (2009). *High-friction devices*.
- R28 Roberts E W, L. S. (2001). *Advanced Tribology Desgin Tools for Space Machanisms*. Warrington, UK.
- R29 Roberts E W, L. S. (2002). *Friction measurements on PEEK 5000* .
- R30 Rossoni P., C. C. (2004). *Deployment Mechanism for the Space Technology 5 Micro Satellite*. Proc 37th Aerospace Mechanisms Symposium, NASA/CP-2004-212073.
- R31 So Young H., N. R. (2015). *Experiment and Numerical Study of Wear in Cross Roller Thrust Bearings*.
- R32 Wardzinski B. (2014). *Friction of Material Pairings*. ESA-ESTL-TM-0133.

Figure 1: ESA Member States and Cooperating States. Credit: European Space Agency 4

Figure 2: LSS brackets. Credit: European Space Agency 5

Figure 3: CAD model of HSCS 1st generation. 5

Figure 4: CAD model of HSCS 2st generation..... 5

Figure 5: HSCS dismounted. Credit: European Space Agency 6

Figure 6: HSCS 2st generation. Credit: European Space Agency 6

Figure 7: ESTEC’s Test Centre. Credit: European Space Agency..... 7

Figure 8: LSS artist’s impression. Credit: European Space Agency 8

Figure 9: Xenon arc lamp solar simulator. Credit: G2Voptics..... 9

Figure 10: LSS Collimation Mirror. Credit: European Space Agency..... 10

Figure 11: Adhesive wear phenomenon. Credit: [R5]..... 14

Figure 12: Output of a general wear measurement. Credit: [R1]. 16

Figure 13: Output of a general friction measurement. Credit: [R1].17

Figure 14: Generic tribometer set up.17

Figure 15: Pin-on-disc setup. Credit: [R31] 18

Figure 16: Two-disc setup. 18

Figure 17: Four-ball setup. [R20] 18

Figure 18, preliminary concept of the joint.20

Figure 19: Employment of the long cylindrical bracket. a. MGSE connected to the LSS (on the left) b. MGSE placed on a flat surface (on the right)..... 26

Figure 20: Employment of the short cylindrical bracket. 27

Figure 21: Dimension of the cylindrical brackets. 27

Figure 22: Schematisation of load on the spherical joint..... 28

Figure 23: Vespel friction coefficient compared to other polymers. Credit: DuPont..... 29

Figure 24: Cross section of spherical joint and friction forces.....30

Figure 25: Cross section of spherical force and applied force.30

Figure 26: Cross section of spherical joint at T=293.15K. 32

Figure 27: Inner ring in Vespel SP3..... 32

Figure 28: Cross section of spherical joint at T=100 K. 34

Figure 29: Spherical joint and support parts: exploded view. 35

Figure 30: Spherical joint and support parts: overall dimentions.....36

Figure 31: Eternal Case. 37

Figure 32: Spherical joint section. 37

Figure 33: Bottom Plate. 37

Figure 34: Bottom Plate Radii dimensions. 38

Figure 35: Sphere. 38

Figure 36: Inner Ring..... 39

Figure 37: Cylindrical Bracket. 39

Figure 38: FoV of the camera. 40

Figure 39: Camera Support.....40

Figure 40: Installation, phase 1: insertion of the Inner Ring on the Sphere. 41

Figure 41: Installation, phase 2, 3 and 4: Completion of the Spherical Joint. 41

Figure 42: Installation, phase 5: Connection with the Camera Support. 42

Figure 43: Installation, phase 6: Fixing of the position. 42

Figure 44: Nominal dimensions. 42

Figure 45: External Case for analysis 44

Figure 46: Display of mesh settings.....44

Figure 47: constraints and load. 45

Figure 48: Translation displacement of External Case under 1N load. 45

Figure 49: Manufacturing of inner ring. 47

Figure 50: Manufactured parts: before and after anodization.	47
Figure 51: LIVAF.	48
Figure 52: test set up.	48
Figure 53: Insulator section.	50
Figure 54: Test in ambient atmosphere: on the left the component at the beginning of the test, on the right the component 24 hours later.	50
Figure 55: Close up of figure 52.	51
Figure 56: Installation of thermocouples and display of the camera set up.	51
Figure 57: Test temperature cycles.	52
Figure 58: Measurement points graph.	53
Figure 59: Pressure drop during the first hour of the test.	54
Figure 60: On the left, Spherical joint in ambient temperature and atmosphere. T1 On the right, Spherical joint in ambient temperature and vacuum (3.28e-6 mbar). T2.	54
Figure 61: Points T3, T4 and T5 (from left to right).	55
Figure 62: Points T6, T7 and T8 (from left to right).	55

Table 1: Unlubricated Wear Rates and Friction Coefficients for Various Materials (in air, crossed cylinders test configuration).

Credit: [R1].	15
Table 2: High friction material coupling possibilities.	19
Table 3: Vespel SP3 main properties.	21
Table 4: Material trade-off.	22
Table 5: Justification of the material trade-off.	22
Table 6: Functional and Performance Requirements.	24
Table 7: Interface Requirements.	24
Table 8: Environmental Requirements.	25
Table 9: Design Requirements.	25
Table 10: Data and results of preliminary calculations.	28
Table 11: Kinetic friction coefficients of Vespel SP3 versus carbon steel, in steady state, unlubricated, in air environment, thrust bearing.	29
Table 12: Definition of parameters to calculate the torque to apply on the bolt.	31
Table 13: Function explanation of each component.	36
Table 14: Bill of Material and mass.	36
Table 15: Tolerances.	43
Table 16: Maximum and minimum play for the spherical joint.	43
Table 17: Function explanation of each component and BoM.	49
Table 18: Thermocouples position.	51
Table 19: Test Details.	52
Table 20: Measurement points table.	53

Annex A : Drawings

